



## 저작자표시 2.0 대한민국

이용자는 아래의 조건을 따르는 경우에 한하여 자유롭게

- 이 저작물을 복제, 배포, 전송, 전시, 공연 및 방송할 수 있습니다.
- 이차적 저작물을 작성할 수 있습니다.
- 이 저작물을 영리 목적으로 이용할 수 있습니다.

다음과 같은 조건을 따라야 합니다:



저작자표시. 귀하는 원저작자를 표시하여야 합니다.

- 귀하는, 이 저작물의 재이용이나 배포의 경우, 이 저작물에 적용된 이용허락조건을 명확하게 나타내어야 합니다.
- 저작권자로부터 별도의 허가를 받으면 이러한 조건들은 적용되지 않습니다.

저작권법에 따른 이용자의 권리는 위의 내용에 의하여 영향을 받지 않습니다.

이것은 [이용허락규약\(Legal Code\)](#)을 이해하기 쉽게 요약한 것입니다.

[Disclaimer](#) 

The role of cochlin LCCL domain  
regulating innate immune cells  
heterogeneity and bacterial clearance  
in peritonitis-derived mouse

Young Ho Choe

Department of Medicine

The Graduate School, Yonsei University

The role of cochlin LCCL domain  
regulating innate immune cells  
heterogeneity and bacterial clearance  
in peritonitis-derived mouse

Directed by Professor Young-Min Hyun

The Doctoral Dissertation  
submitted to the Department of Medicine,  
the Graduate School of Yonsei University  
in partial fulfillment of the requirements for the degree  
of Doctor of Philosophy in Medical Science

Young Ho Choe

December 2023

This certifies that the Doctoral  
Dissertation of Young Ho Choe is  
approved.

-----  
Thesis Supervisor : Young-Min Hyun

-----  
Thesis Committee Member#1 : Je-Wook Yu

-----  
Thesis Committee Member#2 : Minsoo Kim

-----  
Thesis Committee Member#3: Chang Ook Park

-----  
Thesis Committee Member#4: Sung Ho Park

The Graduate School  
Yonsei University

December 2023

## ACKNOWLEDGEMENTS

2017년 1월부터 2024년 초까지 총 7년이라는 긴 시간 동안 여러 국제학회지 논문 게재와 박사학위논문 지도에 큰 도움을 주신 현영민 교수님께 감사의 말씀을 올립니다. 그리고 힘든 시간을 함께 나누고 격려해 주신 부모님과 다른 전공의 대학원이지만 비슷한 시기에 학위 생활을 같이하며 저에게 여러 조언을 해주었던 여동생 예림이에게도 감사의 말을 전합니다. 또한 7년이라는 길다면 길고 짧다면 짧았던 시간 동안 만났던 수많은 연구자분과 랩 구성원들에게도 고마웠다는 말을 전하고 싶습니다. 특히, 들어온 지 얼마 되지 않았지만, 매사에 열정적이고 깎듯한 막내 해랑 선생님과 진득하고 묵묵하게 열심히 일하는 해성이, 늘 유쾌하고 밝은 성격의 기은이, 하나를 가르쳐주면 힘들어도 끝까지 최선을 다해서 결과를 얻어내고 함께 뿌듯함을 느꼈던 현서와 여러 업무와 실험에도 성실하게 역할들을 수행한 경령에게도 감사의 말을 전합니다. 도움과 조언이 필요할 때 언제든지 이야기하며 학위 생활의 절반 이상을 함께 보냈던 재호, 그리고 실험실 입학

동기이자 가장 긴 시간 동안 실험실 생활을 함께하며 여러 추억을 쌓아왔던 소이에게도 감사했다는 말을 전하고 싶습니다. 마지막으로 호탕하고 쾌활한 성격으로 실험실에 긍정적인 에너지를 넘치게 해 주신 김보라 박사님과 앞으로의 진로와 관련하여 좋은 말씀을 많이 해 주셨던 박춘선 박사님께도 큰 감사의 말씀을 드립니다. 이외에 정신적으로 육체적으로 힘든 시기에 다시 일어날 수 있게 해주고 활력을 불어넣어 주었던 많은 친구들과 제 박사학위 논문을 잘 마칠 수 있도록 여러 조언을 아끼시지 않았던 유제욱 교수님, 박창욱 교수님, 김민수 교수님, 그리고 박성호 교수님께도 큰 감사의 말씀을 올립니다. 학위를 마치고 나서 새로운 환경에서 새로운 시작을 하게 될 때 제 학위 기간에 가이드가 되어 주셨던 수많은 분을 가슴에 새기며 나아가도록 하겠습니다. 제 박사학위를 축하해주신 많은 분께 다시 한번 감사의 말씀을 전합니다.

2023 년 12 월

최영호 올림

## <TABLE OF CONTENTS>

<b>ABSTRACT</b> .....	<b>ix</b>
<b>I. INTRODUCTION</b> .....	<b>1</b>
<b>II. MATERIALS AND METHODS</b> .....	<b>4</b>
1. Mice .....	4
2. Two-photon intravital microscopy (TPIVM) .....	4
3. Bacteria culture and transformation .....	6
4. Infection derived peritonitis model .....	7
5. Protein extraction and western blotting .....	8
6. Cytokine array .....	9
7. Organ failure analysis .....	10
8. Flow cytometry .....	10
9. Cytospin for Diff-Quik staining .....	11
10. Single-cell RNA sequencing .....	11
11. RNA extraction and polymerase chain reaction (PCR) .....	13
12. Imaging data analysis .....	15
13. Statistical analysis .....	15
<b>III. RESULTS</b> .....	<b>18</b>
Chapter 1. Application of two-photon intravital microscopy (TPIVM) in research .....	18

1.1. Visualization of immune cell migration in mice liver .....	18
1.2. Stability analysis of bioorganic chemical for visual tracking during intravital imaging .....	20
Chapter 2. Role of cochlin LCCL peptide in LPS-induced sepsis model .....	23
2.1. Expression of proinflammatory genes and proteins increases after systemic inflammation in WT mice .....	23
2.2. Neutrophil infiltration is not altered between WT and Coch KO mice, but cochlin LCCL peptide affects the adhesion of extravasated neutrophils in tissues .....	27
Chapter 3. Function of cochlin LCCL peptide regulating innate immunity in <i>E.coli</i> -derived peritonitis .....	32
3.1. The clearance of bacteria at early time points leads to the accumulation of cochlin LCCL peptide in the peritoneal cavity .....	32
3.2. Cochlin LCCL peptide accelerates a proinflammatory state resulting in increased mortality through a cytokine storm .....	36
3.3. Cochlin LCCL peptide deficiency causes impaired infiltration of monocyte derived macrophages following an infection .....	41
3.4. Gender-specific differences can affect homeostasis and inflamed condition in PECs .....	44

3.5. Transcriptomic analysis showed that ENG <sup>high</sup> neutrophil infiltration to peritoneal cavity significantly increased in Coch KO mice .....	51
3.6. Neutrophils from ENG <sup>low</sup> clusters that express <i>Cxcr2</i> accumulate in the peritoneal cavity, which is induced by cochlin LCCL peptide .....	57
3.7. CXCR2 <sup>high</sup> neutrophil infiltration to the peritoneal cavity of WT mice exacerbates the inflammatory condition compared to Coch KO mice .....	62
<b>IV. DISCUSSION</b> .....	<b>64</b>
<b>V. CONCLUSION</b> .....	<b>69</b>
<b>REFERENCES</b> .....	<b>70</b>
<b>ABSTRACT (IN KOREAN)</b> .....	<b>80</b>
<b>PUBLICATION LIST</b> .....	<b>82</b>

## LIST OF FIGURES

Figure 1. Liver intravital imaging set-up and representative image of neutrophils and macrophages in the liver .....	19
Figure 2. Fluorescence intensity and stability measurement of hydroxycoumarin conjugated dextran in various organs .....	21
Figure 3. mRNA expression of pro-inflammatory genes in spleen and bone marrow are diminished in Coch KO mice after <i>salmonella</i> LPS injection .....	24
Figure 4. Immune cell migration related cytokines and chemokines were decreased in Coch KO mice after <i>salmonella</i> LPS stimulation .....	26
Figure 5. Overall neutrophil infiltration in various tissues was not changed after systemic inflammation in both WT and Coch KO mice .....	28
Figure 6. Adhesion of neutrophils in omentum was increased by cochlin LCCL peptide after <i>E.coli</i> LPS injection .....	31

Figure 7. Cochlin LCCL peptide was accumulated in peritoneal exudate cells (PECs) and bacterial clearance was delayed at early time points after DH5 $\alpha$  infection ..... 33

Figure 8. Phagocytosis was less efficiently performed in peritoneal cavity from Coch KO mice than WT mice after DH5 $\alpha$  infection ..... 35

Figure 9. WT male mice show a higher susceptibility to mortality after DH5 $\alpha$  infection ..... 37

Figure 10. Pro-inflammatory cytokines inducing cytokine storms are down-regulated in Coch KO male mice after DH5 $\alpha$  infection ..... 38

Figure 11. Organ failures are attenuated in Coch KO male mice after DH5 $\alpha$  infection ..... 40

Figure 12. Recruited macrophages are further decreased in Coch KO male mice after DH5 $\alpha$  infection ..... 42

Figure 13. LPMs of Coch KO male mice are significantly reduced in homeostasis ..... 45

Figure 14. Gating strategy of pHrodo red *E.coli* bioparticle engulfed PECs and PECs in non-infected and DH5 $\alpha$  infected condition for cell death analysis ..... 46

Figure 15. Phagocytosis of LPMs and SPMs is not affected by LCCL peptide and gender, but apoptosis of LPMs in WT female mice is alleviated after systemic inflammation ..... 47

Figure 16. Neutrophils from Coch KO female mice show impaired phagocytosis, while necrotic cell death is elevated in WT female mice after systemic inflammation ..... 49

Figure 17. Single-cell RNA sequencing reveals heterogeneity among neutrophils between WT and Coch KO male mice after DH5 $\alpha$  infection ..... 52

Figure 18. Early neutrotime genes (ENGs) are up-regulated in the peritoneal neutrophils of Coch KO male mice after DH5 $\alpha$  infection ..... 55

Figure 19. Peritoneal neutrophils of ENGs low cluster from WT male mice exhibit higher expression of *Cxcr2* after DH5 $\alpha$

infection .....	58
Figure 20. Neutrophils with high expression of CXCR2 are dominant in WT male mice 24 hours after DH5 $\alpha$ infection ...	60
Figure 21. Infiltrated peritoneal neutrophils from WT male mice cause NETosis 24 hours after DH5 $\alpha$ infection .....	63

## LIST OF TABLES

Table 1. Primer lists of RT-PCR .....	16
Table 2. Primer lists of qRT-PCR .....	17

## ABSTRACT

### **The role of cochlin LCCL domain regulating innate immune cells heterogeneity and bacterial clearance in peritonitis-derived mouse**

Young Ho Choe

*Department of Medical Science*

*The Graduate School, Yonsei University*

(Directed by Professor Young-Min Hyun)

The peritoneum and peritoneal cavity are essential barriers that protect organs from external infections. In the peritoneal cavity, various resident immune cells float to detect foreign materials. Once a bacterial infection or inflammation occurs due to trauma, resident macrophages clear the pathogens, and innate immune cells are recruited for additional processes. In this process, numerous anti-bacterial molecules are involved in peritoneal immunity. Among them, cochlin is known to be expressed in the inner ear and vestibule, but it has recently been found to also exist in secondary lymphoid organs such as the spleen and lymph nodes. Cochlin is cleaved to LCCL domain (cochlin LCCL

peptide) after systemic inflammation and secreted into the blood stream. However, the function of the cleaved LCCL peptide in innate immunity is still not fully elucidated. In this study, I found that LCCL peptide plays a crucial role in early phagocytosis as well as the regulation of proinflammatory cytokines. However, LCCL peptide leads to increased mortality caused by organ failure due to prolonged cytokine storm. Using single-cell RNA sequencing, I discovered that early neutrotome genes (ENGs) are up-regulated in Coch KO peritoneal neutrophils. ENGs exhibit a phenotype characterized by immature neutrophils, which includes the *Chil3*, *Camp*, *Mmp8*, and *Ngp* genes. In this study, peritoneal neutrophils of Coch KO mice were less inflammatory and have reduced production of neutrophil extracellular traps (NETs). On the contrary, peritoneal neutrophils from WT mice have a significant population that displays a proinflammatory feature by reacting to CXCL1 and CXCL2 via CXCR2. In conclusion, LCCL peptide recruits CXCR2<sup>high</sup> neutrophils to eliminate bacteria, but this recruitment can also lead to host damage.

---

Key words : cochlin, lccl domain, innate immunity, neutrophil, macrophage, peritonitis, escherichia coli, infection, single-cell RNA sequencing, neutrophil extracellular trap

**The role of cochlin LCCL domain regulating innate immune cells  
heterogeneity and bacterial clearance in peritonitis-derived mouse**

Young Ho Choe

*Department of Medical Science*

*The Graduate School, Yonsei University*

(Directed by Professor Young-Min Hyun)

## **I. INTRODUCTION**

Intestinal microbial infection due to the abdominal trauma, peritoneal dialysis and appendicitis can cause a severe systemic inflammation<sup>1-5</sup>. Those symptoms can lead to peritoneal tissue damage and encapsulating peritoneal sclerosis in the case of severe fibrosis<sup>6-8</sup>. In the worst case, intestinal obstruction can occur, leading to death from abdominal distension and digestive problems<sup>9,10</sup>. In this process, an appropriate immune response of immune cells is essential to

overcome microbial infection and autoimmune disease by various substances<sup>11,12</sup>.

Cochlin protein known as one of the extracellular matrix (ECM) proteins, which is generated mainly in the inner ear and produced in the secondary lymphoid organs such as spleen and lymph nodes, will be investigated in this study<sup>13,14</sup>. It is known that N-terminal of cochlin protein is partially cleaved with aggrecanase I during inflammation and then the truncated domain LCCL peptide flows along the blood stream<sup>13</sup>. It has been also reported that the LCCL peptide moves to the site of infection and helps to induce immune cells to eliminate bacteria in the cochlea, lung, and skin<sup>13-15</sup>. However, the correlation between the LCCL peptide and immune cells in peritoneal cavity has not yet been clarified, and a controllable mechanism has not been established. In the previous study, bacterial infection of peritoneal cavity was rapidly cleared by large peritoneal macrophages (LPMs) and then many neutrophils from the omentum enter through the high endothelial venules (HEVs) to the abdominal cavity<sup>16-18</sup>. In the process of phagocytosing bacteria, control mechanism of neutrophil infiltration by cochlin LCCL peptide has not been demonstrated.

To validate these details, I performed cytokine measurements and assessed immune cell infiltration in the peritoneal cavity after infection, in order to validate cochlin LCCL peptide dependent changes. Furthermore, two-photon intravital imaging was conducted in the omentum to clarify the migration pattern of immune cells. Since the function of cochlin LCCL peptide can

influence whole cells, transcriptome approaches were employed in this study. As mentioned above, single-cell RNA sequencing, one of the transcriptome analyses, was proceeded to confirm the effect of cochlin LCCL peptide on inflammatory peritoneal cavity in the individual cell level. In order to comprehend the genetic characteristics of cell-to-cell interaction during infection, it is necessary to investigate the genetic changes induced by the cochlin LCCL peptide. Based on the interpretation of gene signature of single cell levels, it is expected to find the clue for controlling excessive and detrimental immune response such as circulating citrullinated histone H3 (CitH3) known as one of the neutrophil extracellular traps (NETs) proteins<sup>19,20</sup>. Combining the above, this study aims at investigating the relation between LCCL peptide and innate immune cell regulation by using peritoneal infection model of *E.coli*. Through the single-cell RNA sequencing and mechanism study, I provide evidence to elucidate the mechanism of immune response by cochlin LCCL peptide to identify therapeutic target for systemic inflammatory response such as sepsis.

## II. MATERIALS AND METHODS

### 1. Mice

8-12 weeks of female and male C57BL/6 mice were purchased from Orientbio (Seongnam, Korea) and used for WT control mice. To define function of cochlin *in vivo* and *in vitro*, C57BL/6 background cochlin deficient Coch<sup>-/-</sup> mice (Strain name : B6.129S1(Cg)-Coch<sup>tm1.1Stw</sup>/YuanJ) were kindly provided by professor Jinsei Jung. LysM<sup>GFP/GFP</sup> mice were originally provided from professor Pilhan Kim (KAIST) and heterozygote mice (LysM<sup>GFP/+</sup>) were used for visualizing neutrophils and some monocytes<sup>21</sup>. For cochlin study, LysM<sup>GFP/GFP</sup>;Coch<sup>-/-</sup> mice and Coch<sup>-/-</sup> mice were crossed to deliver LysM<sup>GFP/+</sup>;Coch<sup>-/-</sup> mice. Mice were maintained in specific pathogen-free condition animal facility. All of procedures were conducted in accordance with the guidelines of the Institutional Animal Care and Use Committee (IACUC) of Yonsei University College of Medicine and listed on animal research proposal (IACUC No. 2022-0116) by professor Young-Min Hyun.

### 2. Two-photon intravital microscopy (TPIVM)

Two-photon intravital microscopy was conducted to visualize biomolecules and cell mobility *in vivo* using various organ imaging techniques. For inducing systemic inflammatory condition, 10 mg/kg of *Salmonella* LPS (Sigma-Aldrich, Burlington, Massachusetts, USA) or 2.5 mg/kg of *E.coli* LPS

(Sigma-Aldrich) was intraperitoneally injected. Mice were anesthetized with 30 mg/kg of zoletil 50 (Virbac, Carros, France) and 10 mg/kg of rompun (Bayer, Leverkusen, Germany). Prior to calvarial bone marrow and brain exposure surgery, the head skin was cut. Especially brain exposure surgery was proceeded after drilling skull and fixing cover glass to the hole. A metal ring was attached to the skull with dental resin to allow lens immersion in water. For liver, omentum and cremaster imaging, hair removal of abdomen or scrotum was performed before tissue exposure. Approximately 10mm of a small incision was made under aseptic conditions to expose the liver and omentum. The left lateral lobe of the liver or the entire omentum was mounted on the silicone pedestal. In cremaster muscle imaging, cremaster muscle was pulled out from the scrotum and fixed with insect pin on silicon pedestal. All imaging procedure were conducted on each custom imaging chamber. Prior to conducting the imaging, 25 mg/kg of 70 kDa Texas red conjugated dextran (Invitrogen, Waltham, Massachusetts, USA) or 25 mg/kg of 70 kDa Hydroxycoumarin conjugated dextran or 50  $\mu$ g of CF405M conjugated wheat germ agglutinin (WGA) (Biotium, Fremont, California, USA) were intravenously injected to visualize blood vessels. Body temperature of mice was maintained by heating plate at 37°C. Zen 2010 Black edition (Carl Zeiss, Baden-Württemberg, Germany) was used for setting the laser of LSM 7MP (Carl Zeiss) with optimal power and the wavelength was tuned between 800 nm and 880 nm depending on its purpose. With W Plan-Apochromat 20 $\times$ /1.0

water immersion lens, 3D images (512×512 pixels) were taken at a depth of 40–50  $\mu\text{m}$  with 1  $\mu\text{m}$  slice and for a total of 30 minutes to 1 hour at 60 seconds intervals. Emission filter information; DAPI/SHG, 420–480 nm; GFP/Alexa488, 500–550 nm; and RFP/Alexa 555, 575–610 nm. FVMPE (Olympus, Tokyo, Japan) was used to visualize omentum with water immersion objective for multi-photon 25x/1.05, W.D 2.0mm.

### **3. Bacteria culture and transformation**

DH5 $\alpha$  (*Escherichia coli* strain) was cultured in Luria-Bertani (LB) broth and LB agar plate [Sodium Chloride 10 g (Duksan, Ansan, Korea), Bacto™ Tryptone 10 g (BD Bioscience, San Jose, California, USA), Bacto™ Yeast Extract 5 g (BD Bioscience), Bacto™ Agar 15 g (BD Bioscience) only in agar plate at 1 L of distilled water]. For infection model and microscopic imaging, EGFP-pBAD vector (kindly provided by professor Sangsun Yoon) was transformed to DH5 $\alpha$ . 50  $\mu\text{l}$  of aliquoted DH5 $\alpha$  in -80°C deep freezer was slowly thawed on ice and 80 ng of EGFP-pBAD vector (20  $\mu\text{g}/\text{ml}$ ) was gently mixed with DH5 $\alpha$ . Mixture of DH5 $\alpha$  and EGFP-pBAD vector was incubated on ice for 30 minutes. For heat shock of DH5 $\alpha$ , mixture tube was placed into a 42°C water bath for 60 seconds and put the tube back on ice for 3 minutes. LB broth without antibiotics was added to mixture about 900  $\mu\text{l}$  and mixture was incubated in 37°C shaking incubator for 1 hour. 100  $\mu\text{l}$  of incubated sample was spread and grown in 100  $\mu\text{g}/\text{ml}$  ampicillin supplemented LB agar plate in

37°C incubator for overnight. Single colony of DH5 $\alpha$  was cultured in 100  $\mu$ g/ml ampicillin supplemented LB broth in 37°C shaking incubator for stock freezing and infection.

#### **4. Infection derived peritonitis model**

For inducing peritonitis with bacteria,  $1 \times 10^8$  colony forming unit (CFU) of ampicillin resistance DH5 $\alpha$  in 200  $\mu$ l 1X PBS was injected into peritoneal cavity avoiding intestine injection. CFU for infection was calculated with serial dilution via optical density (OD) 600 nm reached at 1. CFU/ml was calculated with following formula. [Colony numbers x Dilution factor / Loading volume (ml)]. Infection was maintained from 0 to 24 hours and mice were sacrificed for further experiments. Survival of mice was observed at 24 hours interval and mice were sacrificed at 96 hours after infection. To analyze phagocytic ability of peritoneal immune cells, 200  $\mu$ g of pHrodo red *E.coli* bioparticles (Invitrogen) in PBS were intraperitoneally injected to mimic bacterial infection model. pHrodo red *E.coli* bioparticles were sonicated and vortexed before injection.

## 5. Protein extraction and western blotting

Peritoneal exudate cells (PECs) were harvested by peritoneal lavage fluid (PLF) injecting with 5 ml of ice-cold PBS. Peritoneum of mice was strongly massaged with several times to collect adhesive cluster of cells. For protein extraction, whole PECs were lysed without enzyme digestion. In case of using neutrophil of PECs, neutrophils were isolated by neutrophil negative selection kit (Miltenyi Biotec, Bergisch Gladbach, Germany) with manufacturer's protocol. Isolated cells were directly incubated with RIPA lysis and extraction buffer (Thermo Scientific, Waltham, Massachusetts, USA) containing 1X Xpert protease inhibitor cocktail (GenDEPOT, Houston, Texas, USA) and 1X Xpert phosphatase inhibitor cocktail (GenDEPOT) for 30 minutes on ice with vortexing. Supernatant was collected with spin down of lysed PECs at 13,000 rpm for 10 minutes at 4°C. For collecting serum, mouse blood was isolated via cardiac puncture. Blood was clotted for 30 minutes at room temperature. Serum was isolated with centrifugation at 2,000 g for 10 minutes at 4°C. Concentration of lysates and sera was measured by bicinchoninic acid (BCA) assay. Samples were diluted at 5X sample loading buffer containing DTT (Tech & Innovation, Chuncheon, Korea) and boiled for 5 minutes at 95°C heat block. 10 and 12% gel were used for western blotting. SDS-PAGE was conducted with 1X running buffer about 2 hours. 0.2 µm size PVDF membrane was activated with methanol prior to transfer. Transfer was performed for 1 hour on ice. Membrane was blocked for 1 hour at room temperature with 5%

non-fat skim milk in 1X TBST (0.1% tween 20). Rat anti-mouse cochlin mAb (Merck, Darmstadt, Germany) (1:1000), Rat anti-mouse chil3 mAb (Biolegend, San Diego, California, USA) (1:1000), Rabbit anti-mouse CitH3 pAb (Abcam, Cambridge, UK) (1:1000), Rabbit anti-mouse MPO mAb (Abcam) (1:1000), and Rabbit anti-mouse  $\beta$ -actin mAb (Cell Signaling Technology ; CST, Danvers, Massachusetts, USA) (1:2500) were diluted into antibody dilution buffer (5% skim milk, 0.02% sodium azide containing 1X TBST). 1<sup>st</sup> antibody was blotted with shaking incubation for overnight at 4°C. Membrane was washed with 1X TBST and rat or rabbit-anti mouse IgG pAb with HRP conjugate was used for 2<sup>nd</sup> antibody blotting. After washing membrane, Clarity Max ECL (Bio-Rad, Hercules, California, USA) (1:1) or SuperSignal™ West Atto Ultimate Sensitivity Substrate (Thermo Scientific) (1:1) was used for low expressed protein develop. Westsave up ECL (Abfrontier, Seoul, Korea) (1:200) was used for developing membrane with high expressed protein samples.

## 6. Cytokine array

To measure LCCL peptide dependent cytokine expression level of sera, Proteome Profiler Mouse Cytokine Array Kit panel A (R&D Systems, Minneapolis, Minnesota, USA) was used. For inducing systemic inflammation, 10 mg/kg of *Salmonella* LPS or  $1 \times 10^8$  CFU of DH5 $\alpha$  was intraperitoneally injected. All procedure was followed by manufacturer's instruction. After

incubation of included ECL, membranes were developed with X-ray film in dark room. Then, films were scanned and analyzed with HImage++ software (Ideal Eyes Systems, Bountiful, Utah, USA). All value was normalized with positive and negative control for calculating pixel density.

### **7. Organ failure analysis**

Isolated serum was used to measure level of aspartate aminotransferases (AST), alanine aminotransferase (ALT), lactate dehydrogenase (LDH), and urea. All procedure was conducted with ALT/GPT, AST/GOT, LDH activity assay kit and urea (BUN) colorimetric assay kit (Elabscience, Houston, Texas, USA) by manufacturer's instrument. Optical density of each assay was measured by plate spectrophotometer (Epoch, Tokyo, Japan).

### **8. Flow cytometry**

Bone marrow cells were isolated from femur and tibia by flushing with FACS buffer [1X PBS with 2% FBS (Welgene, Gyeongsan, Korea) and 2 mM EDTA (Invitrogen)]. Blood cells were harvested by EDTA coated syringe via cardiac puncture. Spleen cells were collected by mincing tissues and filtering through 70  $\mu$ m size strainer. PECs were enzymatically digested with enzyme digestion solution 1 [RPMI 1640 with 20 mM HEPES (Sigma-Aldrich), 1% fatty acid free BSA (Gibco, Waltham, Massachusetts, USA), 0.05 mg/ml Liberase TL (Roche, Basel, Switzerland), and 0.25 mg/ml DNase I

(Sigma-Aldrich)]. For single cell isolation of PECs, 200  $\mu$ l of enzyme digestion solution was used to incubate for 3 minutes at 37°C heat block. After enzymatic digestion, FACS buffer was used for stopping digestion. Red blood cells were lysed by ACK lysing buffer (Gibco) using osmotic pressure. Before immunostaining of samples, 40  $\mu$ m size strainer was used for removing cell clump and debris. 1  $\mu$ g of FcR (CD16/32) blocking antibody (93, Biolegend) was used prior to fluorescent antibody incubation for 10 minutes at 4°C. 0.5  $\mu$ g of FITC-Ly6G (1A8, Biolegend), 0.5  $\mu$ g of BV421-CXCR4 (L276F12, Biolegend), 0.2  $\mu$ g of BV421-MHCII (M5/114.15.2, Biolegend), 0.2  $\mu$ g of PE-F4/80 (BM8, Biolegend), 0.2  $\mu$ g of APC-CD11b (M1/70, Biolegend), 0.2  $\mu$ g of BV711-F4/80 (BM8, Biolegend), 0.5  $\mu$ g of Alexa fluor 700-F4/80 (BM8, Biolegend), 0.5  $\mu$ g of PE/Cy7-CXCR2 (SA044G4, Biolegend), and 0.2  $\mu$ g of APC/Cy7-Ly6G (1A8, Biolegend), were incubated for 30 minutes at 4°C for each staining strategies. Stained samples were washed with FACS buffer twice and fixed with 4% formaldehyde for 10 minutes at 4°C. Viability assay of peritoneal neutrophil was conducted by FITC-Annexin V (Biolegend) and DAPI (Invitrogen) staining with manufacturer's instruments. Flow cytometry was conducted with LSRII, LSRFortessa, and FACSymphony A5 (BD Bioscience). Raw data of flow cytometry was analyzed by FlowJo v10.2 (BD Bioscience).

## 9. Cytospin for Diff-Quik staining

Isolated fresh PECs were centrifugated with 2,000 rpm for 10 minutes at 4°C. Prior to stain samples, 40 µm size strainer was used for removing large cell clumps and debris. Then, PECs were counted with hemocytometer for optimal density.  $5 \times 10^5$  of PECs were loaded to funnel and cytocentrifugated with 1,000 rpm for 3 minutes at room temperature. For Diff-Quik staining, cell covered slide was dried at room temperature for 5 minutes and fixed with methanol-based fixative in Diff-Quik staining kit (Biozoa, Seoul, Korea). Fixed cell was superfused with solution A and solution B with manufacturer's protocol. After all procedure, slide was mounted with Eprexia Shandon synthetic mountant (Eprexia, Kalamazoo, Michigan, USA) for bright field microscopy. Diff-Quik stained slide samples were imaged by BX53 upright microscope (Olympus).

## 10. Single-cell RNA sequencing

Single-cell RNA sequencing was performed with single cells of PECs 4 hours after DH5α infection. Isolated cells were stained by 0.5 µg of PerCP-CD45 mAb (30-F11, Biolegend) for flow cytometry associated cell sorting (FACS). Viability of CD45<sup>+</sup> PECs were measured by trypan blue staining and AO/PI staining. Over 80% viability of cells were loaded for library. Each cell suspension was subjected to 3' single-cell RNA sequencing using the Chromium Next GEM Single Cell 3p RNA library v3.1 (10x

Genomics, Pleasanton, California, USA). Libraries were sequenced on HiSeq platform (Illumina, San Diego, California, USA) and mapped to mm10 (GENCODE vM23). The gene expression matrices generated by the Cell Ranger toolkit were analyzed on Seurat (v 4.3.0; <https://satijalab.org/seurat/>). Additionally, cells with <200 detected genes, and cells with >10% of mitochondrial genes were filtered. Artificial doublets were detected and removed using DoubletFinder (version 2.0.3; <https://github.com/chris-mcginnis-ucsf/DoubletFinder>) with the developer's guidelines. The Seurat package's built-in function was used to visualize the dimension reduction plots, violin plots, heat map plots, and feature plots. Cell population plots and scatter plots of differentially expressed genes were visualized by the ggplot2 package (v 3.4.0).

## **11. RNA extraction and polymerase chain reaction (PCR)**

RNA extraction of bone marrow, blood, and PECs derived neutrophils were proceeded by TRIzol reagent (Invitrogen) method. Neutrophils from bone marrow, blood, and PECs were isolated by histopaque 1.077 and 1.119 (Sigma) at 872 x g of centrifugation for 30 minutes in room temperature without brake. Neutrophil fraction was collected at between histopaque 1.119 and 1.077 phase without red blood cell depletion. Isolated neutrophils were directly incubated in 1 ml of TRIzol reagent with griding. Samples were incubated for 5 minutes and 200  $\mu$ l of chloroform (VWR, Randor,

Pennsylvania, USA) was added for 3 minutes at room temperature. RNA, DNA, lipid, and protein fraction were isolated 15 minutes after 13,000 rpm of centrifugation at 4°C. 400 µl of aqueous phase of RNA and iso-propanol (Biosesang, Yongin, Korea) were mixed at 1:1 ratio with inverting. After 10 minutes of incubation, pellets of samples were collected by 13,000 rpm of centrifugation at 4°C. Pellets were washed with 75% ethanol and resuspended in ultra-pure distilled water (Invitrogen). Concentration of RNA was measured by nanodrop, and cDNA synthesis was proceeded with AccuPower® CycleScript™ RT PreMix containing oligo dT primer (Bioneer, Daejeon, Korea) followed by manufacturer's protocol. RT-PCR was used to validate RNA expression levels of WT and Coch KO mice with band thickness in agarose gel. To amplify interested gene, 2X Taq PCR Master Mix (BioFACT, Daejeon, Korea) was used. The final PCR product and 100 bp DNA ladder (Bioneer) were loaded onto an agarose gel containing 1xTAE buffer and run using gel electrophoresis. Quantitative real-time PCR was conducted with mixture of TB Green® Premix Ex Taq™ II (Takara, Kyoto, Japan), primers, and cDNA. All samples were loaded on optical reaction 96-well plate with triplicates. PCR reaction was conducted with Quantstudio3 Real-Time PCR System (Applied biosystems, Foster City, California, USA). To measure relative expression level of interested gene,  $\Delta\Delta C_t$  method was used. All primers used for gene amplification was listed on Table 1 and 2.

## **12. Imaging data analysis**

All two-photon intravital imaging data were analyzed with Volocity v6.3.1 (Quorum, Ontario, Canada) or Imaris v7.2.3 (Bitplane, Belfast, UK). For adjusting contrast of image and measuring cell motility of video, volocity software was used. On the contrary, Imaris was used for rendering fluorescence image to 3D. In cytospin slide samples of bright field imaging, extracellular bacteria were manually counted with Image J (N.I.H, Bethesda, Maryland, USA) software.

## **13. Statistical analysis**

Statistical analysis was performed with Prism v7.0 (GraphPad, San Diego, California, USA). For comparing with two or more samples, student's t-test, or one-way ANOVA with post-hoc test was conducted. All values were tested for normality, and the Mann-Whitney's U, Kruskal-Wallis test was conducted after normal distribution was not followed. Grouped samples were analyzed by two-way ANOVA with post-hoc test.

**Table 1. Primer list of RT-PCR**

Gene	Forward primer (5'-3')	Product size (bp)
	Reverse primer (5'-3')	
<i>Tbp</i>	GAGTTGCTTGCTCTGTGCTG	164
	CTGGCTTGTGTGGGAAAGAT	
<i>Coch</i>	GACAAGGCTGTGTGTCGGAA	171
	GGAGCCGTCAATCAGAAAGG	
<i>Adamts4</i>	CAGACGAAGCACTCACCTTG	180
	CACAAGTCCTGGAGCAGTCA	
<i>Infg</i>	GCTTTGCAGCTCTTCCTCAT	162
	GTCACCATCCTTTTGCCAGT	
<i>Cxcl1</i>	GCTGGGATTCACCTCAAGAA	169
	TGGGGACACCTTTTAGCATC	
<i>Cxcl2</i>	CAGACTCCAGCCACACTTCA	132
	CAGTTCACTGGCCACAACAG	
<i>Cxcl10</i>	GGATGGCTGTCCTAGCTCTG	107
	TGAGCTAGGGAGGACAAGGA	
<i>Il6</i>	GTCCTTCCTACCCCAATTTCCA	154
	TAACGCACTAGGTTTGCCGA	

**Table 2. Primer list of qRT-PCR**

Gene	Forward primer (5'-3')	Product size (bp)
	Reverse primer (5'-3')	
<i>Tbp</i>	GAGTTGCTTGCTCTGTGCTG	164
	CTGGCTTGTGTGGGAAAGAT	
<i>Chil3</i>	TCCACAGTGCATTCTGCATC	118
	CCAGCTGGTACAGCAGACAA	
<i>Camp</i>	GTCTTGGAACCATGCAGTT	146
	TGGTTGAAGTCATCCACAGC	
<i>Mmp8</i>	AAACGGAGTGAGAGGTGTGG	143
	CCCTCCAGTGTCTGGTTCTC	
<i>Ngp</i>	GTCCATTTGCTTCCTTCTGC	145
	GAACTGATGTGGGCAGGACT	

### III. RESULTS

#### Chapter 1. Application of two-photon intravital microscopy (TPIVM) in research

##### 1.1. Visualization of immune cell migration in mice liver

Up to now, various approaches for visualizing tissue to cell or cell to cell interaction were utilized such as immunohistochemistry and tissue clearing. However, those techniques were fixed time image that cannot analyze real-time interaction of cells. To overcome those limitations, two-photon intravital microscopy has shed light in recent years. I set up the aseptic liver intravital imaging technique different from other groups<sup>22</sup>. Left lateral lobe of liver was pulled out from the abdomen and fixed with tissue glue to silicone pedestal for imaging (Figure 1A). Maintaining anesthetize, liver intravital imaging can be continued until 4 hours (Figure 1B). Using this technique, neutrophils and macrophages in the liver can be traced in real-time manner. In my results, liver neutrophils from 10 mg/kg of salmonella LPS injected mice were more infiltrated and adhesive than PBS injected control mice (Figure 1C). In addition, I visualized liver capsular macrophages in the surface of liver that distinguished from monocytes in sinusoids (Figure 1D). These results indicate that two-photon intravital microscopy of liver has an advantage for immune cell trafficking with less photo damage.

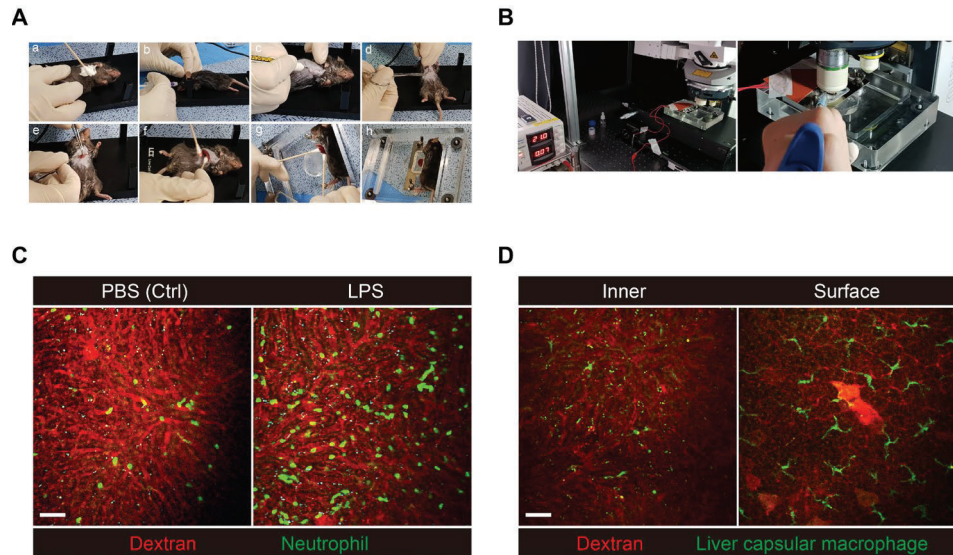
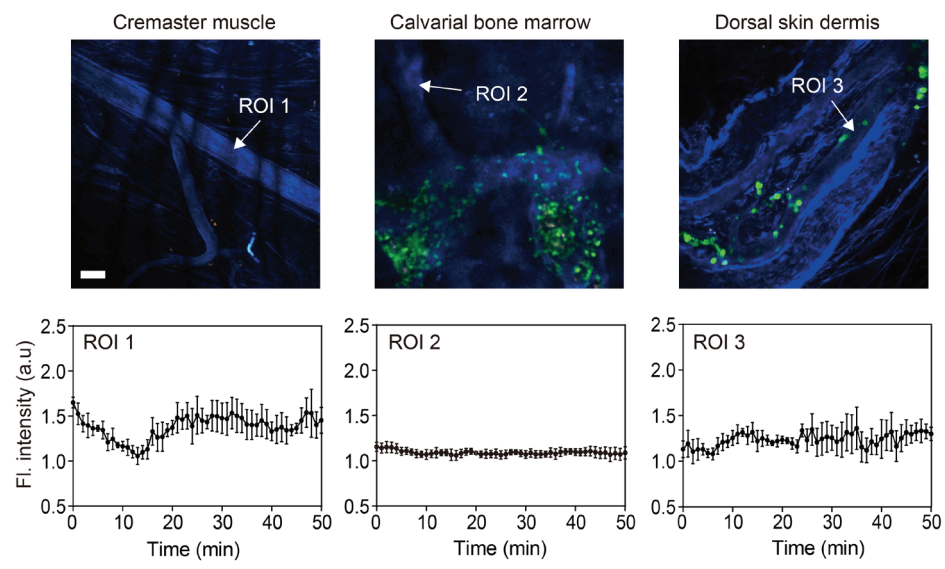


**Figure 1. Liver intravital imaging set-up and representative image of neutrophils and macrophages in the liver.** (A) Surgery process of liver exposure for intravital imaging in (a) to (h). (B) Representative image of preparing two-photon intravital microscopy. (C) Representative snapshot of liver intravital image using  $LysM^{GFP/+}$  mice 4 hours after PBS (control) and 10 mg/kg of salmonella LPS injection. (D) Representative snapshot of liver intravital image using  $CX_3CR1^{GFP/+}$  mice in normal control. The site of sinusoid was referred to the inner (0 to  $-40 \mu m$ ) and above presented a surface (0 to  $+20 \mu m$ ).

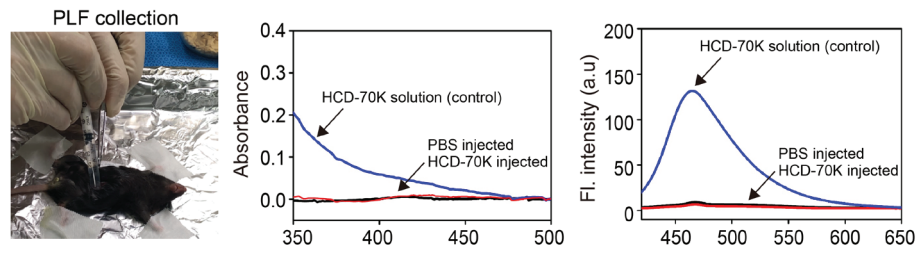
## **1.2. Stability analysis of bioorganic chemical for visual tracking during intravital imaging**

Unlike immune cell tracking in two-photon intravital microscopy, bio-organic molecules can be tested *in vivo*. I used 7-hydroxycoumarin (HDC) conjugated dextran to visualize blood vessels by blue fluorescence in two-photon intravital imaging<sup>23</sup>. 7-hydroxycoumarin excites at 410 nm and emits 464 nm. 7-hydroxycoumarin was conjugated with 70 kDa dextran (HCD-70K) by metal-free biorthogonal click-chemistry. Since 70 kDa dextran was similar to serum albumin (66 kDa) in blood, 70 kDa dextran can be efficiently used for monitoring blood flow in normal condition. I tested the stability of HCD-70K in various organs such as calvarial bone marrow, brain, dorsal dermis, and cremaster muscle. Measuring mean fluorescence intensity (MFI) in the region of interest (ROI), I found that HCD-70K did not leak about 1 hours after injection in different organs (Figure 2A). More specifically, peritoneal lavage fluid was conducted to validate vascular leakage of HCD-70K 30 minutes after injection. Emission of HCD-70K in fluid was not detected compared to control HCD-70K solution (Figure 2B). Moreover, HCD-70K not affected to bleed-through in other fluorescence and motility of immune cells in brain (Figure 2C). Results show that HCD-70K is novel fluorescence molecules with high stability and no toxicity in tissues to combine other fluorescence dye.

**A**



**B**



**C**

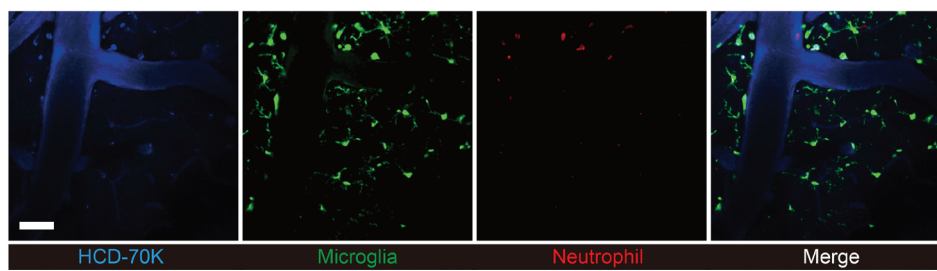


**Figure 2. Fluorescence intensity and stability measurement of hydroxycoumarin conjugated dextran in various organs.** (A) Vascular leakage analysis of various organs (cremaster muscle, calvarial bone marrow, dorsal dermis skin) using two-photon intravital imaging. Fluorescence intensity was measured with each region of interest (ROI). Each ROI was selected at least 3 positions. (B) Absorbance and fluorescence intensity measurement of HCD-70K in control solution and PLF. (C) Representative snapshot of the split channel of brain imaging in CX<sub>3</sub>CR1<sup>GFP/+</sup> mouse. Neutrophils were stained by intravenous injection of 2 μg PE-Ly6G before imaging.

## Chapter 2. Role of cochlin LCCL peptide in LPS-induced sepsis model

### 2.1. Expression of proinflammatory genes and proteins increases after systemic inflammation in WT mice

To define the role of cochlin LCCL peptide in overall tissues, I intraperitoneally injected 10 mg/kg of *salmonella* LPS to WT and cochlin knock out (Coch KO) mice for 4 hours and 24 hours (Figure 3A). First, I validated mRNA expression level of spleen and bone marrow in WT and Coch KO mice. Since spleen is known as cochlin producing organ, I confirmed *coch*, *adamts4* gene expression. As expected, *coch* and *adamts4* expression was highly expressed in WT mice, not Coch KO mice spleen. Especially, *coch* was slightly up-regulated in LPS treated WT mice spleen along with high expression of *adamts4* at 4 hours after injection (Figure 3B). This indicates that cochlin cleavage is actively occurred at 4 hours after LPS injection but reduced at 24 hours after LPS injection (Figure 3B, C). *Coch* expression in bone marrow might be related with replenishing follicular dendritic cell precursor in spleen.

Next, I demonstrated proinflammatory genes inducing immune cell migration and infiltration. Interestingly, the genes *Infg*, *cxcl1*, *cxcl2*, *cxcl10*, and *Il6* were found to be decreased at 4 hours after LPS injection in both the spleen and bone marrow of Coch KO mice, with lower levels observed in the latter. In addition, the expression of only *Infg*, *cxcl1* and *cxcl2* was decreased in Coch KO mice 24 hours after LPS injection. Data shows that

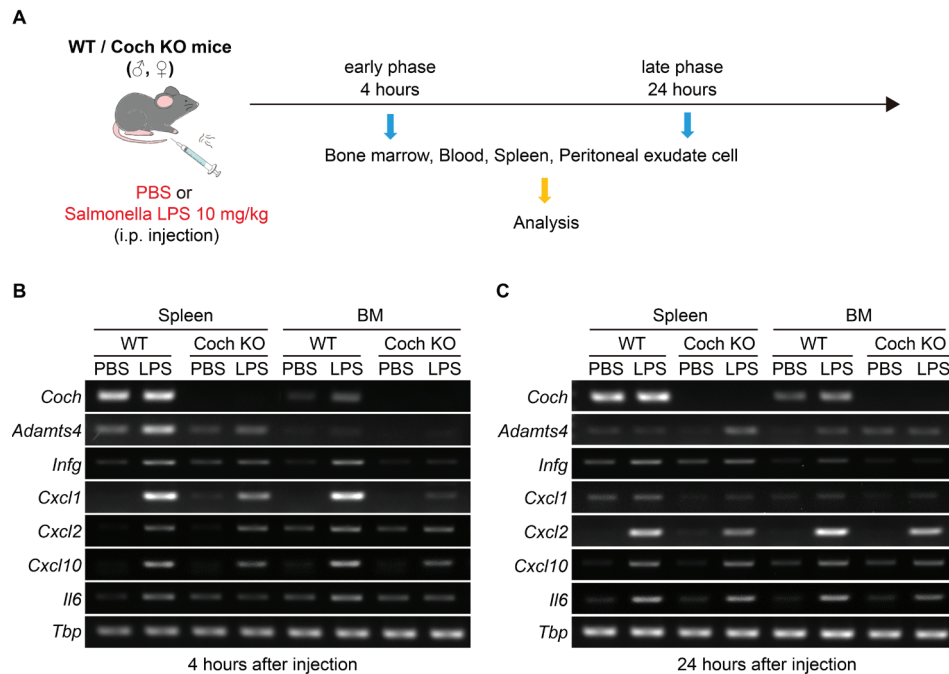


**Figure 3. mRNA expression of pro-inflammatory genes in spleen and bone marrow are diminished in Coch KO mice after salmonella LPS injection.**

(A) Experimental scheme of injection and bone marrow, spleen cell preparation for RNA extraction, RT-PCR and flow cytometry. Bloods were collected for isolating sera and single cells. Peritoneal exudate cells were harvested for flow cytometric analysis. (B) Representative gel image of PCR product 4 hours after injection. (C) Representative gel image of PCR product 24 hours after injection. 1.5% agarose gel was used for electrophoresis. Similar results were obtained 3 times independently.

proinflammatory gene expression patterns are altered at both early and late time points following LPS stimulation. Despite changes, overall proinflammatory gene signatures are diminished in Coch KO mice, indicating that Coch KO mice have difficulty recruiting innate immune cells to tissues.

Then, I validated the protein expression of cytokines and chemokines in sera. IL-6 was highly decreased 4 hours after LPS injection in Coch KO mice. Unlike mRNA expression, CXCL2 was diminished, but CXCL1 and CXCL10 were not altered in Coch KO mice at 4 hours after LPS injection (Figure 4A). On the contrary, IL-6 and CXCL2 expression of sera were abolished at 24 hours after LPS injection in both WT and Coch KO mice. Notably, the levels of CXCL1 and CXCL10 in the sera of Coch KO mice were approximately 2-fold lower than those in WT mice (Figure 4B). Combining the data, results show that cytokines and chemokines involving immune cell infiltration are generally down-regulated in Coch KO mice. In addition, the difference between mRNA and protein levels might be influenced by other cell types in other organs.

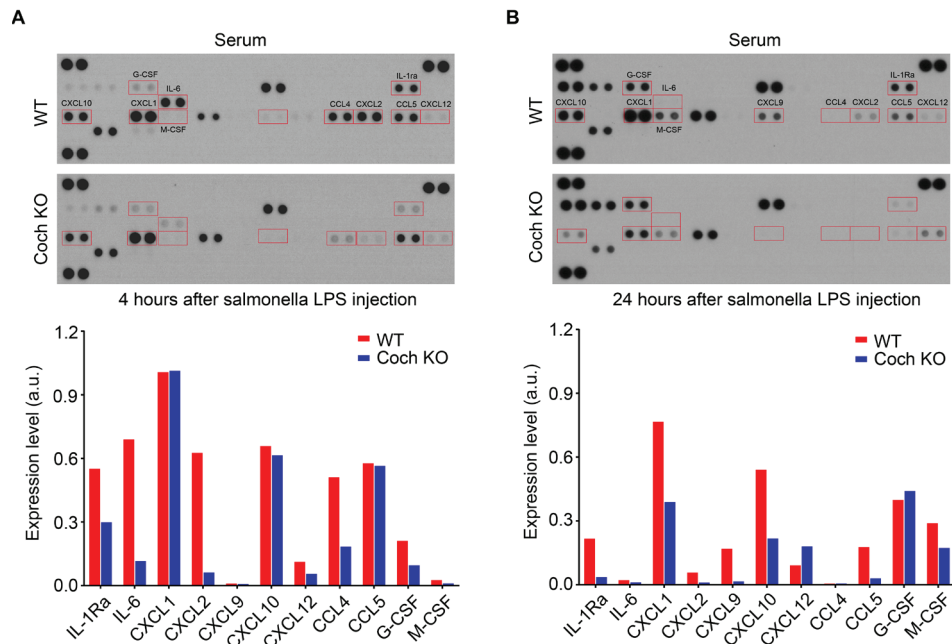


**Figure 4. Immune cell migration related cytokines and chemokines were decreased in Coch KO mice after salmonella LPS stimulation.** (A) Representative snapshot of the cytokine array membrane using WT and Coch KO sera and the relative expression levels of cytokines 4 hours after salmonella LPS injection. (B) Representative snapshot of the cytokine array membrane using WT and Coch KO sera and the relative expression levels of cytokines 24 hours after salmonella LPS injection. The expression levels of the two samples in each condition were averaged.

## **2.2. Neutrophil infiltration is not altered between WT and Coch KO mice, but cochlin LCCL peptide affects the adhesion of extravasated neutrophils in tissues**

In my previous data, I found that the levels of IL-6, CXCL1, and CXCL2 were significantly lower in the sera of Coch KO mice compared to WT mice. Therefore, flow cytometry was performed on bone marrow, blood, spleen, and peritoneal exudate cells to demonstrate the infiltration of neutrophils, which are the first recruited innate immune cells. 24 hours after salmonella LPS injection, there was a slight increase in neutrophils intravasating from the bone marrow to the blood and spleen in Coch KO mice (Figure 5A). However, there were no differences in extravasated peritoneal neutrophils between WT and Coch KO mice. Furthermore, the number of neutrophils in homeostasis did not change in any organs (Figure 5A, B). Through these findings, I hypothesized that there may be more detailed subsets in neutrophils, which could potentially be related to functional differences in tissues.

Next, I confirmed the function of neutrophils in the omentum by utilizing two-photon intravital microscopy. Omentum is a central organ in interaction with the peritoneal cavity. LysM-eGFP mice showed strong green fluorescence protein expression in blood and tissue neutrophils, but a slightly diminished expression of GFP in tissue resident macrophages. The number of extravasated neutrophils from high endothelial venules (HEVs) was no

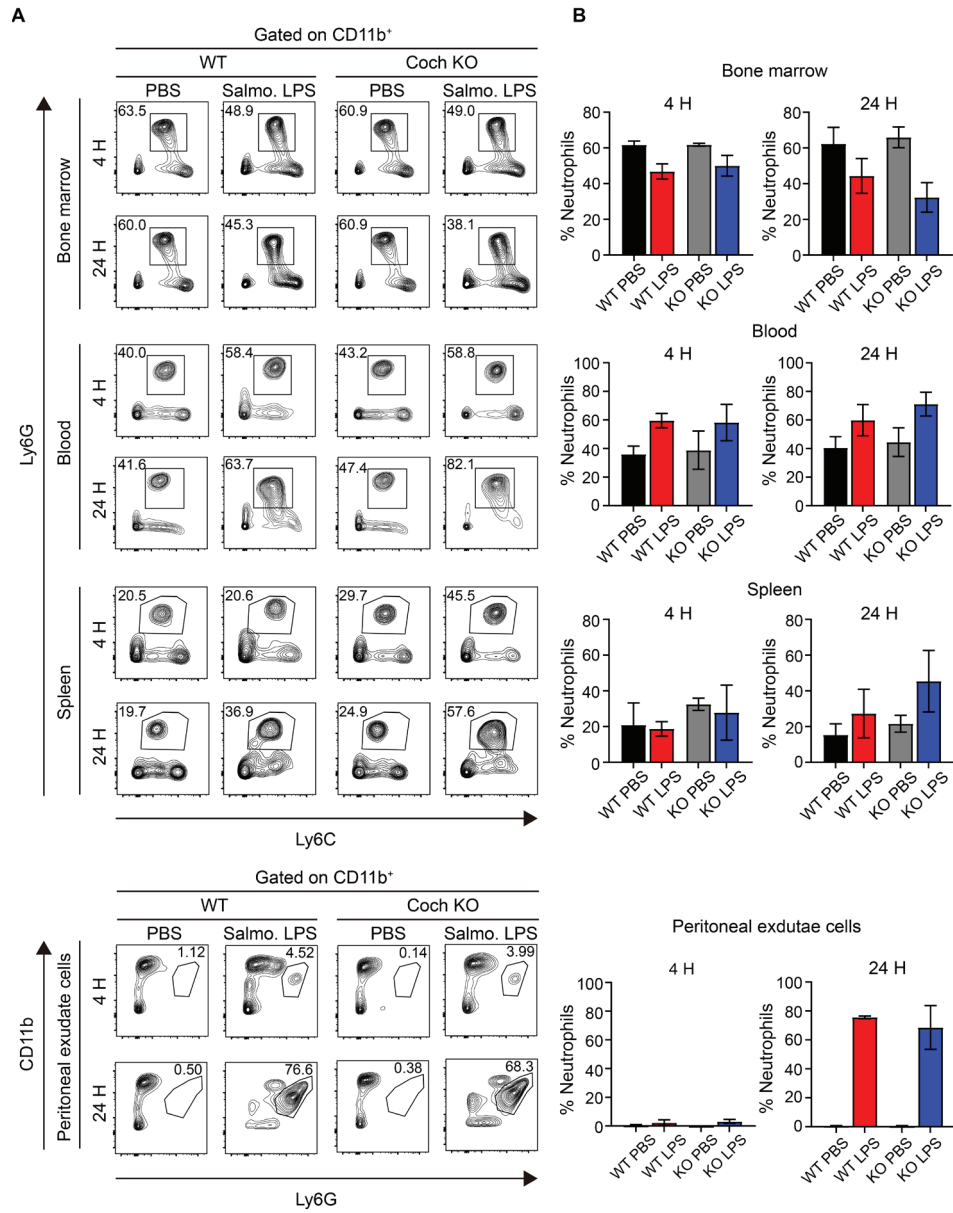


**Figure 5. Overall neutrophil infiltration in various tissues was not changed after systemic inflammation in both WT and Coch KO mice.** (A) Flow cytometry dot plot of neutrophils in bone marrow, blood, spleen, and peritoneal exudate cells. Each gating was defined as non-staining and fluorescence minus one (FMO). (B) The percentage of neutrophils in bone marrow, blood, spleen, and peritoneal exudate cells. At least 3 times were repeated for acquiring data. Statistical analysis was performed by one-way ANOVA.

difference between WT and Coch KO mice after *E.coli* LPS injection (Figure 6A). However, the migratory pattern of neutrophils in interstitial tissues was distinguished by their velocity. Omental neutrophils from Coch KO mice exhibited higher velocity levels compared to WT mice (Figure 6B). There were no differences in displacement rate and meandering index between WT and Coch KO mice. As presented in the snapshot, omental neutrophils from WT mice visualized more adhesive-like structure. From the results, I hypothesized that cochlin LCCL peptide might affect the adhesion of neutrophils in tissues.

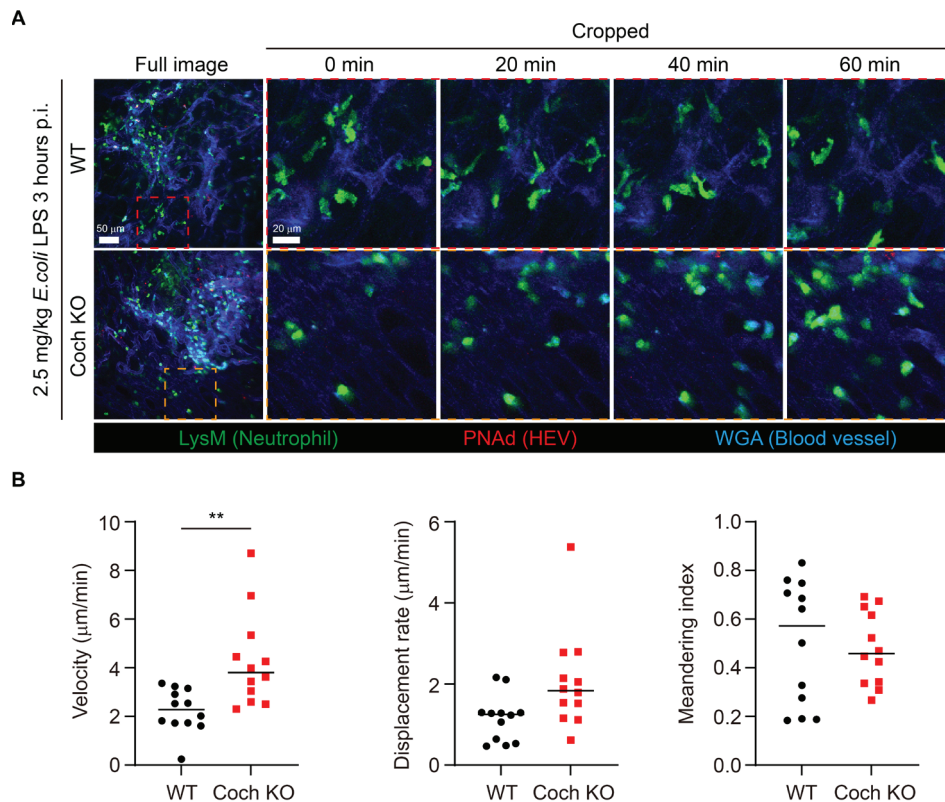


**Figure 6. Adhesion of neutrophils in omentum was increased by cochlin LCCL peptide after *E. coli* LPS injection.** (A) Representative full and cropped snapshot of omentum intravital imaging using Coch<sup>+/+</sup>;LysM<sup>GFP/+</sup> and Coch<sup>-/-</sup>;LysM<sup>GFP/+</sup> mice. (B) Velocity, displacement rate, and meandering index data using manual cell tracking by volocity software. Each dots indicated tracked cells. 3 independent ROIs were selected for analysis. Statistical analysis was performed by Mann-Whitney's U test. *P*-value : \*\* < 0.01.

### **Chapter 3. Function of cochlin LCCL regulating innate immunity in *E.coli*-derived peritonitis**

#### **3.1. The clearance of bacteria at early time points leads to the accumulation of cochlin LCCL peptide in the peritoneal cavity**

To induce systemic inflammatory and infected condition in mice,  $1 \times 10^8$  CFU of DH5 $\alpha$  was injected into peritoneal cavity for 0 hour to 24 hours. Control group was intraperitoneally injected only 1X PBS. After DH5 $\alpha$  infection, I collected sera and PECs of mice to measure cochlin LCCL peptide level in blood and PECs (Figure 7A). Circulating LCCL peptide in blood was dramatically increased at 2 hours to 4 hours and then decreased at 8 hours after infection. However, the circulating LCCL peptide was not detected in Coch KO mice as expected (Figure 7B). On the other hand, the LCCL peptide in PECs of WT mice was observed at 24 hours after infection but not the early timepoints (Figure 7B). This data indicates that the LCCL peptide is rapidly cleaved from spleen derived cochlin and moves to the blood, accumulating in the peritoneal cavity as the inflammatory response goes on.

Then, the effect of LCCL peptide in bacterial clearance at peritoneal cavity was measured by colony forming unit (CFU). As the infection was progressed, bacterial clearance was markedly decreased at 2, 4 hours after infection in Coch KO mice compared to WT mice. However, no difference was observed between WT and Coch KO mice at 8 hours and 24 hours, respectively, after infection (Figure 7C). This result shows that LCCL peptide is related

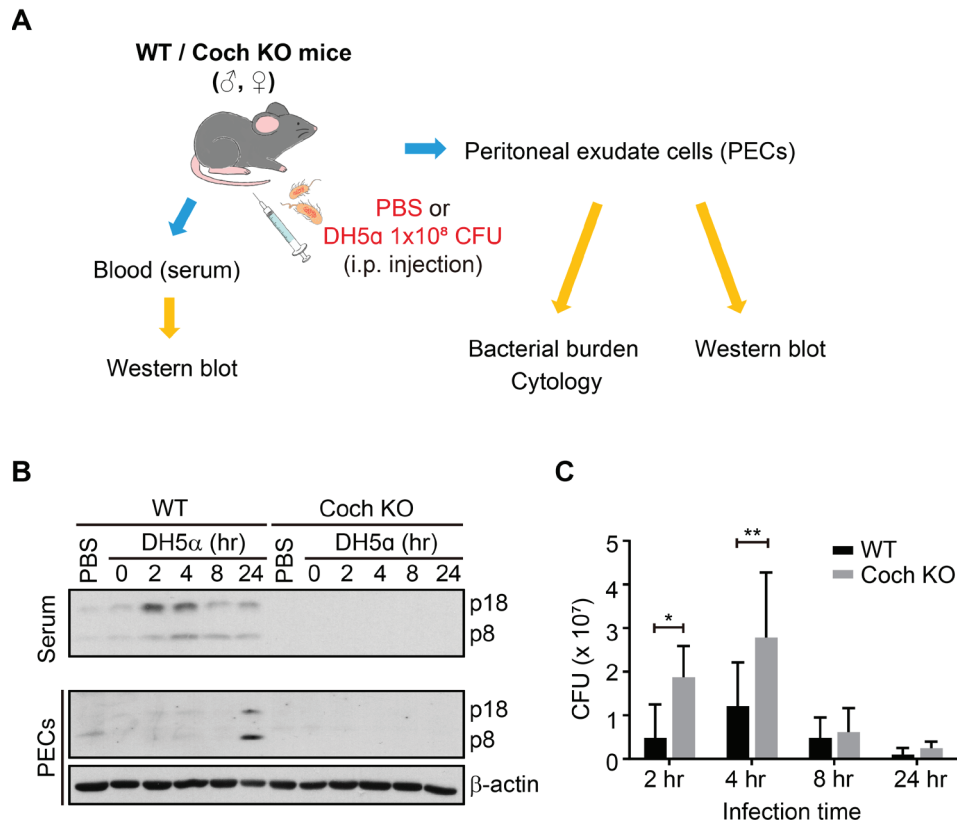


**Figure 7. Cochlin LCCL peptide was accumulated in peritoneal exudate cells (PECs) and bacterial clearance was delayed at early time points after DH5α infection.** (A) Experimental scheme for sample preparation of serum and PECs. (B) Western blotting data of mice serum and PECs was shown in snapshot. 50 μg of serum and 20 μg of PECs lysate were used for sampling. LCCL peptide was composed of two isoforms (18 kDa : Glycosylation form, 8 kDa : Non-glycosylation form). Results were obtained 3 times. (C) Colony forming unit (CFU) of PLF after DH5α infection. Statistical analysis was performed by multiple t-test. *P*-value : \* <0.05 , \*\* < 0.01.

indirectly or directly to clear bacteria at the early phase post infection (~ 4 hours). Since bacterial burden might be related in mortality of mice, I monitored survival of male and female mice after infection.

Using brightfield microscopy, I also confirmed that peritoneal phagocytes more inactively engulfed bacteria in Coch KO mice than WT mice at 30 minutes and 4 hours after infection (Figure 8A). Although peritoneal neutrophils showed less infiltration until 4 hours after infection, they still uptake some bacteria. Manual count data showed that non-phagocytized extracellular bacteria were significantly higher in Coch KO mice than WT mice (Figure 8B). Since lack of LCCL peptide led to less phagocytosis by phagocytes such as LPMs and SPMs in peritoneal cavity, bacterial burden might be higher in Coch KO mice than WT mice (Figure 7C).

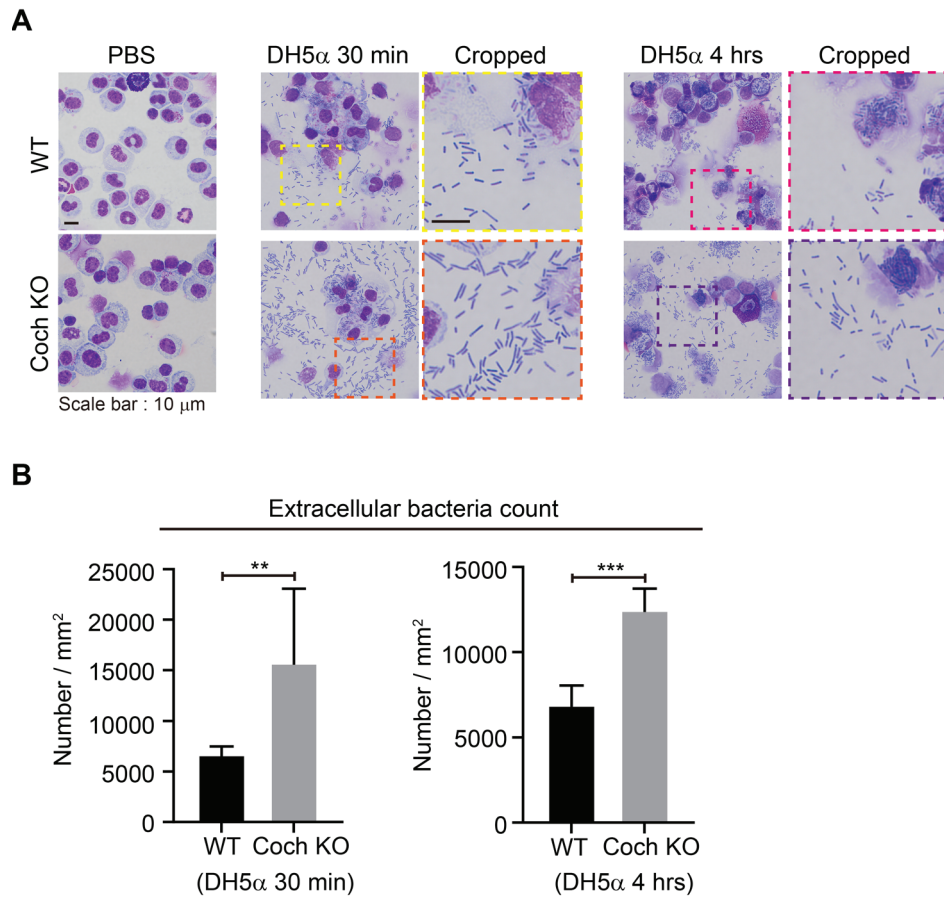


**Figure 8. Phagocytosis was less efficiently performed in peritoneal cavity from Coch KO mice than WT mice after DH5 $\alpha$  infection.** (A) Representative bright field image of cytopsin in non-infected and DH5 $\alpha$  infected PECs. 100X oil immersed lens was used for capturing image. (B) The Image J software was used to count extracellular bacteria for each snapshot. 3 independent ROIs were selected for analysis. Statistical analysis was performed by Mann-Whitney's U test. *P*-value : \*\* < 0.01, \*\*\* < 0.001.

### **3.2. Cochlin LCCL peptide accelerates a proinflammatory state resulting in increased mortality through a cytokine storm**

In the previous studies, immune cell populations in peritoneal cavity have been studied to differ between male and female<sup>24-27</sup>. To demonstrate distinct pattern of cochlin LCCL peptide in gender, survival rate and blood components were monitored after DH5 $\alpha$  infection (Figure 9A). Interestingly, WT male mice were more vulnerable in bacterial infection than Coch KO (Figure 9B). However, both WT and Coch KO female mice had no significant difference in mortality (Figure 9B). Cytokine level of mice sera was measured to validate major cytokines involved in mortality. Several proinflammatory cytokines and chemokines (IL-6, IL-16, CXCL1, CXCL2, CXCL9, CXCL10, CCL5) were significantly decreased in Coch KO male mice (Figure 10A, B). Although IL-1ra is known as antagonist of IL-1 $\alpha$  and  $\beta$ , expression of IL-1ra was increased in WT male mice (Figure 10A, B). IL-1 $\alpha$  and  $\beta$  are representative proinflammatory cytokine expressed by overall immune cells and stromal cells. They mainly interact with endothelial cell to secrete CCL2 and upregulate vascular adhesion molecules such as ICAM-1. In this process, IL-1ra is upregulated to block the function of IL-1 to neutralize inflammation<sup>28,29</sup>. Therefore, this data means that IL-1 $\alpha$  and  $\beta$  are continuously secreted more WT mice sera than Coch KO and IL-1ra is highly expressed to maintain homeostasis.

Combining the cytokine array data, results suggest that WT mice have

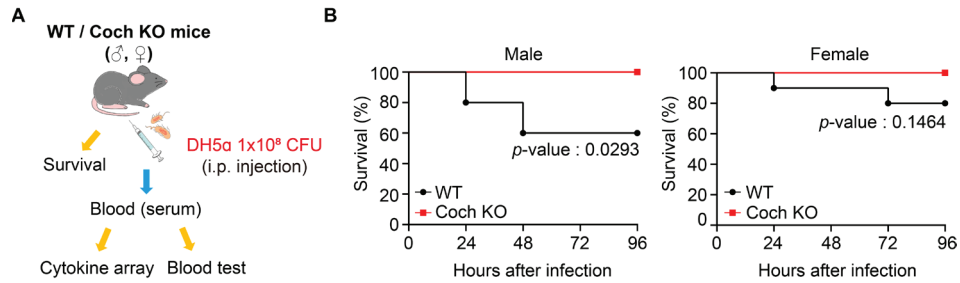


**Figure 9. WT male mice show a higher susceptibility to mortality after DH5 $\alpha$  infection.** (A) Experimental scheme for measuring survival rate and collecting sera for further analysis. (B) Survival rate of WT and Coch KO mice after 1x10<sup>8</sup> CFU DH5 $\alpha$  infection. Infected mice were monitored until recovering health. 10 mice were used for survival test in each condition. Statistical analysis was performed by log-rank test.

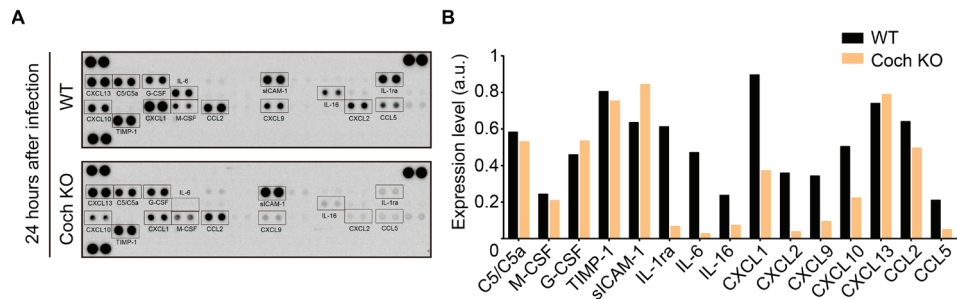


**Figure 10. Pro-inflammatory cytokines inducing cytokine storms are down-regulated in Coch KO male mice after *DH5a* infection.** (A) Snapshot image of cytokine array of sera after infection. The sera of 7 samples from WT and Coch KO mice were pooled. Total 100  $\mu$ g of each serum was loaded to the cytokine array kit. (B) Relative level of cytokine and chemokine expression about cytokine array kit. Highly expressed protein (Black lined box in Figure 10A) was shown in graph. Data was normalized with negative and positive control.

difficulty in stabilizing cytokine levels within 24 hours after infection. In addition, since IL-6, CXCL1 and CXCL2 are the major chemokines for neutrophil infiltration, I checked tissue damage due to excessive immune response of neutrophils. Alanine aminotransferase (ALT), Aspartate aminotransferase (AST), Lactate dehydrogenase (LDH), and Urea level of sera were significantly decreased in Coch KO male mice (Figure 11). This indicates that organ failure of liver, heart, muscle, and kidney are alleviated in Coch KO mice compared to WT mice. This indicates that organ failure of liver, heart, muscle, and kidney are diminished in Coch KO mice compared to WT mice. In these results, I hypothesized that cochlin LCCL peptide can aid early bacterial clearance in both male and female mice, but uncontrollable cytokine storm causes various organ failure in male mice.

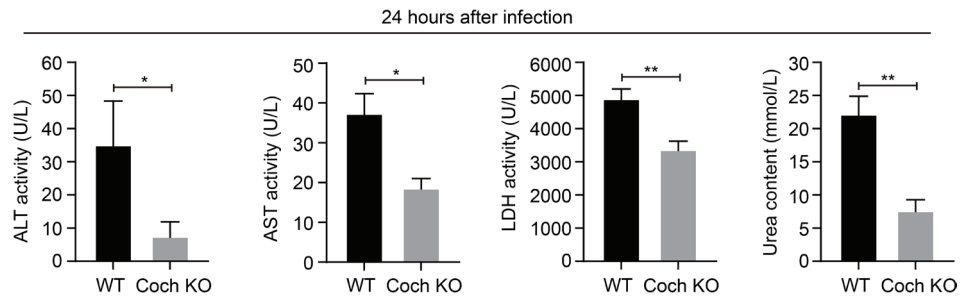


**Figure 11. Organ failures are attenuated in Coch KO male mice after DH5 $\alpha$  infection.** Enzymatic activity and urea contents relating organ failure in sera 24 hours after DH5 $\alpha$  infection. 5 independent experiments were performed for obtaining results. Activity of enzyme was calculated with manufacturer's protocols. Statistical analysis was performed by Mann-Whitney's U test. *P*-value : \* <0.05 , \*\* < 0.01.

### **3.3. Cochlin LCCL peptide deficiency causes impaired infiltration of monocyte derived macrophages following an infection**

To define immune cell distribution at peritoneal cavity after infection, flow cytometry was performed to determine percentage of immune cells in PECs from male and female mice (Figure 12A). Neutrophils were widely known that extravasate from the blood vessel to site of inflammation<sup>30-32</sup>. In my data, neutrophil numbers in PECs of WT and Coch KO mice were not different at 2, 4, 8, 24 hours after infection. However, the infiltrated neutrophils in PECs of Coch KO mice at 8 hours after infection were slightly higher than those in WT mice (Figure 12B).

Unlike neutrophils, there are two types of macrophages in peritoneal cavity. CD11b<sup>+</sup> F4/80<sup>high</sup> macrophages were large peritoneal macrophages (LPMs) and small peritoneal macrophages (SPMs) were included in CD11b<sup>+</sup> F4/80<sup>low</sup> population<sup>33</sup>. In normal condition, LPMs were existed about most of the peritoneal cells (30~50%) but CD11b<sup>+</sup> F4/80<sup>low</sup> populations were in only small portions (~5%) (Figure 12C). However, LPMs were slightly reduced 2 and 4 hours after peritoneal infection in Coch KO mice than WT mice and barely detected both mice after 8 hours to 24 hours (Figure 12C). In the contrast of Coch KO mice, CD11b<sup>+</sup> F4/80<sup>low</sup> population including SPMs were instantaneously increased at 2 hours after infection in WT mice and gradually decreased (Figure 12D). In 2 hours after infection, the recruited population may include inflammatory monocytes and monocytes-derived SPMs,

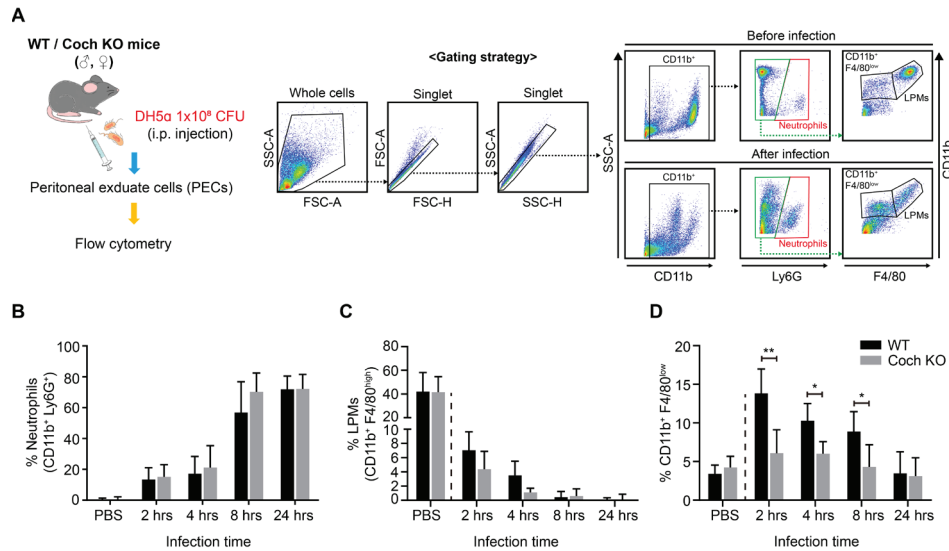


**Figure 12. Recruited macrophages are further decreased in Coch KO male mice after DH5 $\alpha$  infection.** (A) Schematic figure and gating strategy of flow cytometry in PECs from non-infected and infected mice. All samples were gated with FMO samples and negative control. (B) Neutrophil percentage in PECs at different time points. (C) LPMs percentage in PECs at different time points. (D) CD11b<sup>+</sup> F4/80<sup>low</sup> population in PECs at different time points. All samples are gated on singlet. Statistical analysis was performed by multiple t-test. *P*-value : \* <0.05, \*\* <0.01.

characterized by CD11b<sup>+</sup> F4/80<sup>low</sup> expression. Although most of the LPMs undergo pyroptosis and macrophage disappearance reaction (MDR) at peritoneal cavity, remaining bacteria were phagocytosed by LPMs or SPMs and migrated to omentum<sup>18</sup>.

Comprehensively, bacterial clearance in peritoneal cavity was mainly occurred by LPMs and SPMs within 4 hours after infection and neutrophils were recruited from omentum to peritoneal cavity for late phagocytosis (Figure 12B-D). Despite these results, neutrophils of PECs at 4 hours after infection were not different between WT and Coch KO mice (Figure 12B). Therefore, I hypothesized that neutrophils in Coch KO mice are not functioning properly, and this dysfunction may be related to survival outcomes.

### **3.4. Gender-specific differences can affect homeostasis and inflamed condition in PECs.**

In various of previous studies, gender specific differences of peritoneal immune cells are well-established. To validate the different percentage of innate immune cells in PECs, I conducted flow cytometry of WT and Coch KO male and female mice (Figure 13A, 14A). The results showed that the number of LPMs not in female, but Coch KO male mice were significantly lower than that in WT male mice. More specifically, SPMs and monocytes were distinguished by MHC II marker. Monocytes were CD11b<sup>+</sup> MHC II subset, but SPMs expressed CD11b and MHC II with high level. Like SPMs, some neutrophils divided by MHC II after DH5 $\alpha$  infection (Figure 14A). SPMs, monocytes, and neutrophils of PECs in basal level were not influenced by LCCL peptide and gender (Figure 13B). Next, I demonstrated the function of phagocytosis between immune cells from WT and Coch KO male and female mice (Figure 14B, 15A). Engulfed and digested *E.coli* bioparticles were not changed at LPMs and SPMs of WT and Coch KO male and female mice (Figure 15A). However, apoptosis of LPMs from WT female mice showed significant decline (Figure 15B). On the contrary, both necrosis of LPMs and SPMs were no difference between gender, and cochlin dependent manner (Figure 15C). Then, I confirmed the phagocytic ability and cell death of neutrophils in PECs after *E.coli* bioparticle injection and DH5 $\alpha$  infection. The results indicated that neutrophils from Coch KO female mice impaired phagocytosis, not in male mice (Figure 16A). To validate whether bacteria phagocytosed neutrophils undergo cell death, apoptosis and necrosis were

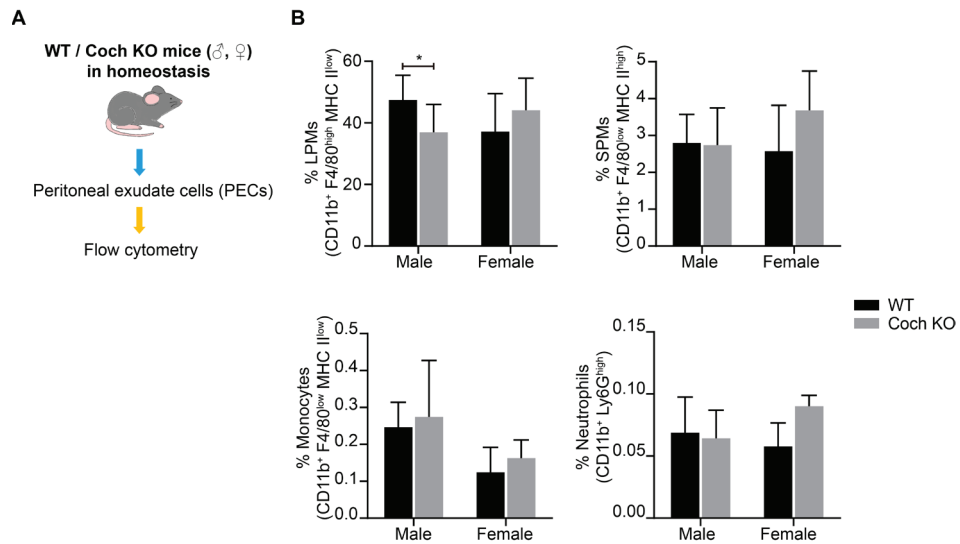


**Figure 13. LPMs of Coch KO male mice are significantly reduced in homeostasis.** (A) Experimental scheme of isolating PECs from WT and Coch KO male and female mice in homeostasis. (B) Percentage of LPMs, SPMs, monocytes, neutrophils were displayed in graph. Statistical analysis was performed by multiple t-test. *P*-value : \* <0.05

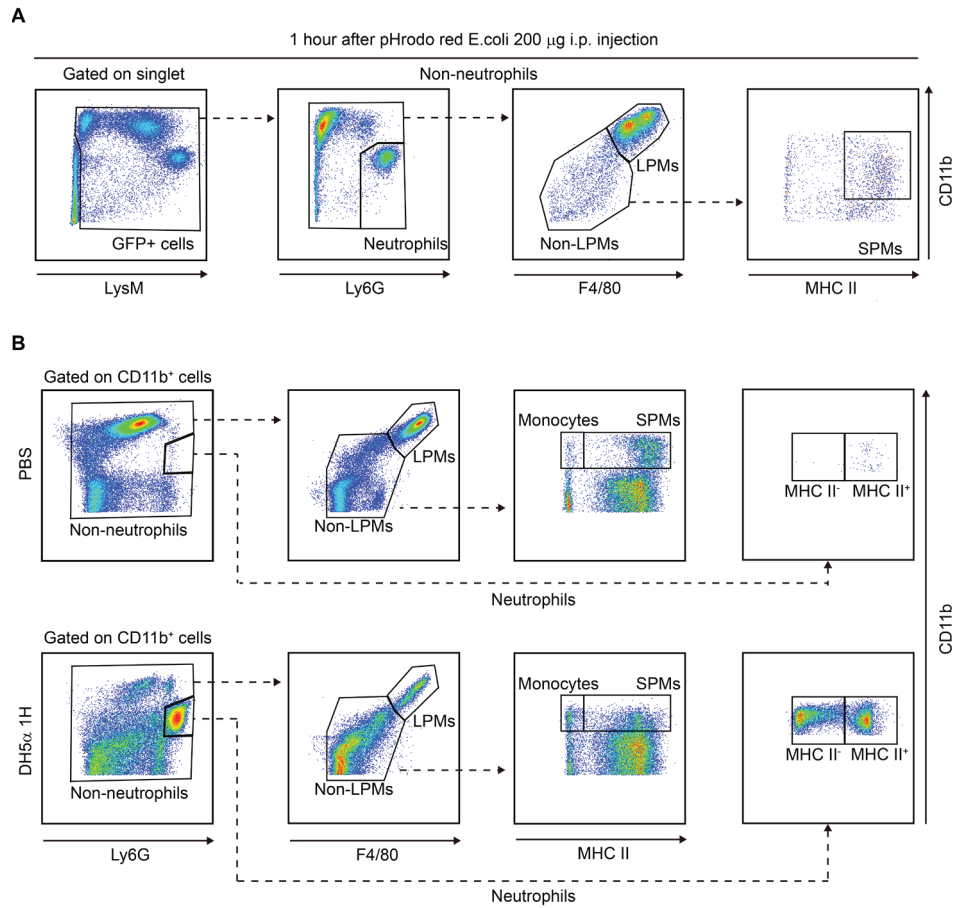


**Figure 14. Gating strategy of pHrodo red *E.coli* bioparticle engulfed PECs and PECs in non-infected and DH5 $\alpha$  infected condition for cell death analysis. (A) Gating strategy of PECs from LysM GFP mice. (B) Gating strategy of PECs in non-infected and infected conditions. All samples are gated on singlet. Total 100,000 singlet was counted in each sample.**

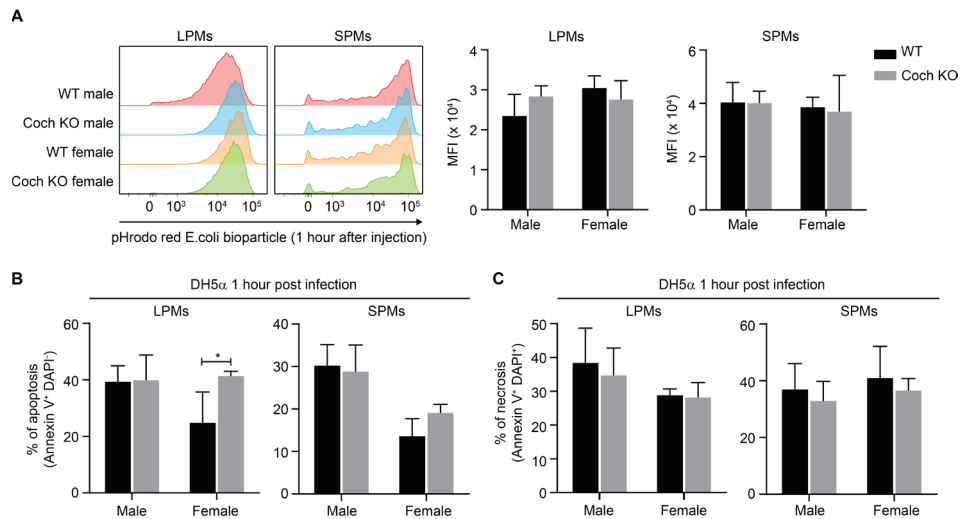


**Figure 15. Phagocytosis of LPMs and SPMs is not affected by LCCL peptide and gender, but apoptosis of LPMs in WT female mice is alleviated after systemic inflammation.** (A) Phagocytosis intensity of pHrodo red *E.coli* bioparticle was displayed by histogram. Mean fluorescence intensity (MFI) was calculated and presented to graph. (B) Percentage of apoptosis in LPMs and SPMs 1 hour after DH5 $\alpha$  infection. (C) Percentage of necrosis in LPMs and SPMs 1 hour after DH5 $\alpha$  infection. Statistical analysis was performed by multiple t-test. *P*-value : \* <0.05.

measured in neutrophils, MHC II<sup>-</sup>, and MHC II<sup>+</sup> neutrophils. Apoptosis of each neutrophil subset was not altered between WT and Coch KO male and female mice (Figure 16B). However, necrosis of MHC II<sup>-</sup> neutrophils from WT female mice was highly elevated than Coch KO male and female mice (Figure 16C). Combining the results, self-renewal function of LPMs may be influenced by cochlin, but not phagocytosis and cell death in macrophages. On the contrary, neutrophils are not affected by cochlin LCCL peptide.

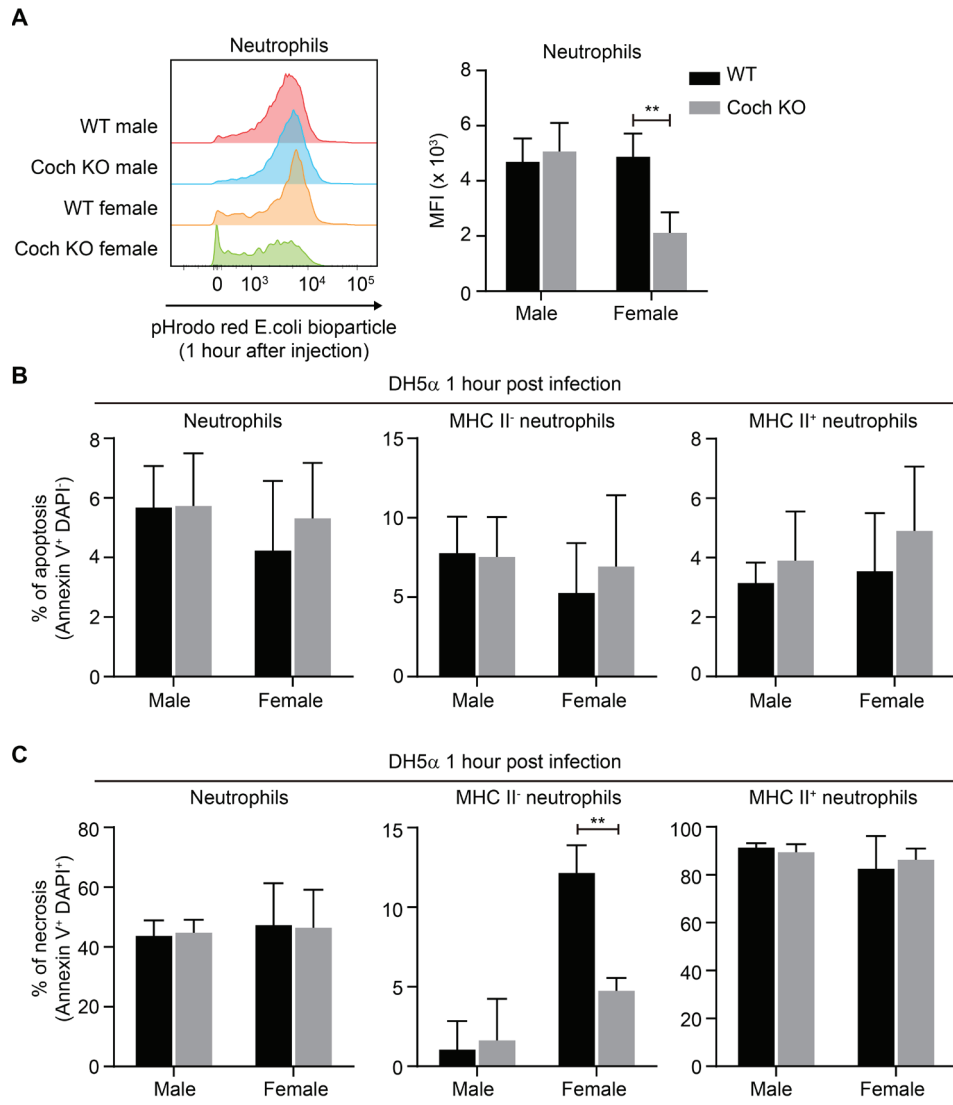


**Figure 16. Neutrophils from Coch KO female mice show impaired phagocytosis, while necrotic cell death is elevated in WT female mice after systemic inflammation.** (A) Phagocytosis intensity of pHrodo red *E.coli* bioparticle was displayed by histogram. MFI was calculated and presented to graph. (B) Percentage of apoptosis in neutrophils, MHC II<sup>-</sup>, and MHC II<sup>+</sup> neutrophils 1 hour after DH5 $\alpha$  infection. (C) Percentage of necrosis in neutrophils, MHC II<sup>-</sup>, and MHC II<sup>+</sup> neutrophils 1 hour after DH5 $\alpha$  infection. Statistical analysis was performed by multiple t-test. *P*-value : \*\* <0.01.

### **3.5. Transcriptomic analysis showed that ENG<sup>high</sup> neutrophil infiltration to peritoneal cavity significantly increased in Coch KO mice**

Next, I performed transcriptome analysis of peritoneal cells with single-cell RNA sequencing to dissect different RNA expression of individual cells. Through isolated peritoneal cells, CD45<sup>+</sup> cells were collected with FACS and analyzed by 10X genomics (Figure 17A). Single-cell RNA sequencing of CD45<sup>+</sup> cells in peritoneal cavity revealed five clusters in my condition (Neutrophils, B cells, Mast cells, NK and T cells, and Macrophages) (Figure 17B). Each cluster was classified with specific gene set (Data not shown). Then, I confirmed the number and ratio of five clusters between WT and Coch KO mice. Interestingly, macrophage population was lower, but B cell population was higher in Coch KO mice than WT mice before infection (Data not shown). However, there are no changes in five subsets between WT and Coch KO mice 4 hours after DH5 $\alpha$  infection (Figure 17B). As a results of this finding, cochlin might be involved in macrophage proliferation and B cell expansion. Since macrophage population was lower in Coch KO mice, bacterial clearance and flow cytometry data were supported by single-cell RNA sequencing.

Early phagocytosis (0 hour to 2 hours) of LPMs was widely known, but LCCL peptide derived immune cell infiltration was not elucidated yet. To define the recruited innate immune cells in PECs, neutrophils were additionally analyzed. Neutrophils are known as one of the fully

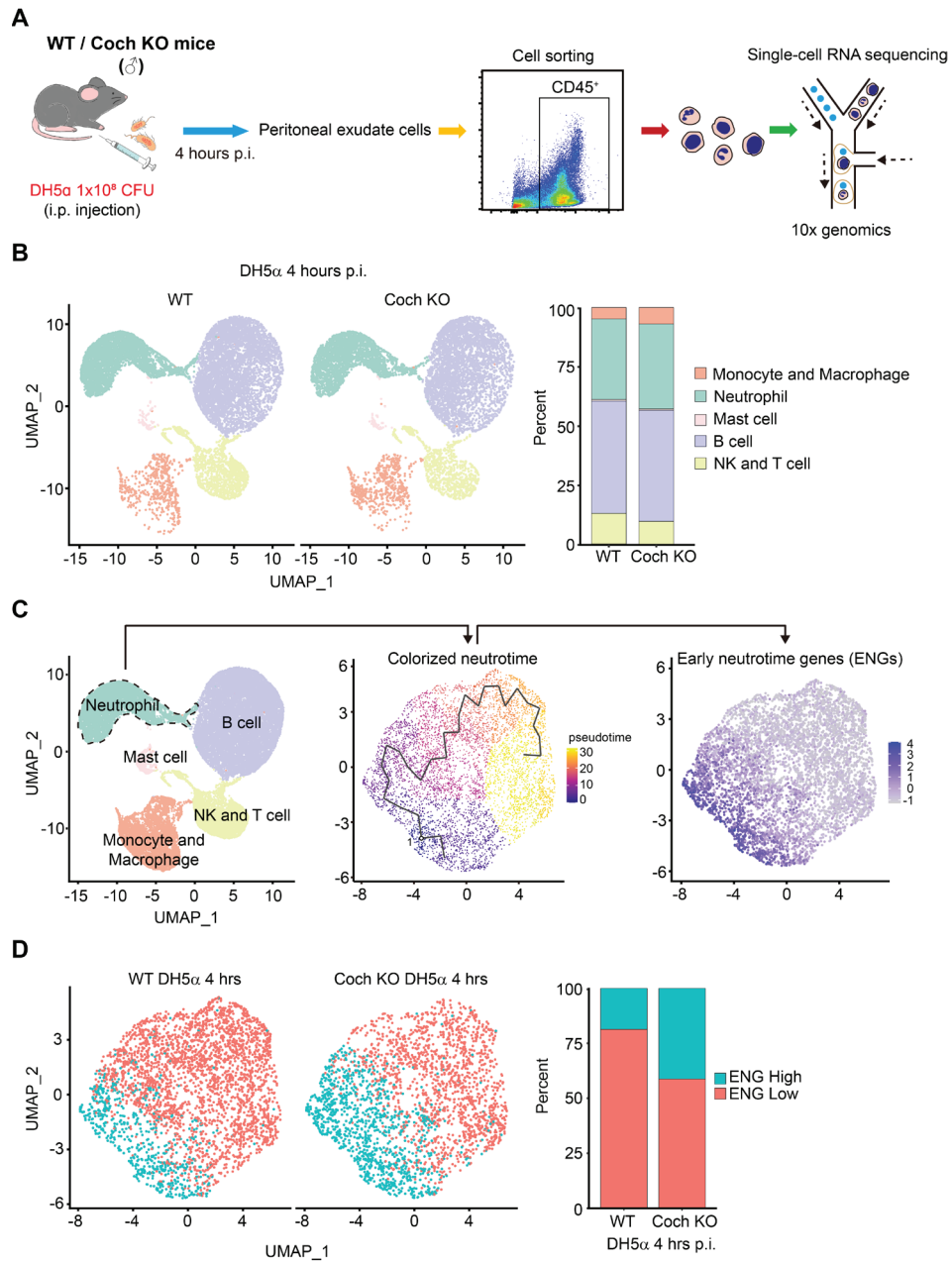


**Figure 17. Single-cell RNA sequencing reveals heterogeneity among neutrophils between WT and Coch KO male mice after DH5 $\alpha$  infection.**

(A) Isolated PECs were sorted by CD45 marker using FACS, and the sorted CD45<sup>+</sup> cells were used for single-cell RNA sequencing on the same day. (B) UMAP projection and percentage for infection group of WT and Coch KO mice in CD45<sup>+</sup> PECs. About 10,000 cells were presented in the plot. (C) Feature plot of ENGs with pseudotime and expression level in peritoneal neutrophils. (D) Comparison for ENG high and low population of peritoneal neutrophils between WT and Coch KO mice.

differentiated cells and the pioneer to the infection site but have various phenotypes at organ and environments<sup>34</sup>. Especially, maturity of neutrophils is determined by several genes controlling function of neutrophils<sup>35,36</sup>.

In systemic inflammatory condition, mature bone marrow neutrophils can intravasate bone marrow to blood for migrating toward the site of infection<sup>37</sup>. I focused on the neutrophil phenotype difference between WT and Coch KO mice. Various of previous studies show that neutrophils have dynamic gene expression by maturation<sup>35,36,38</sup>. Early neutrotime genes (ENGs) are known as highly expressed gene set in mature neutrophil of bone marrow than mature neutrophil of blood<sup>38</sup>. My data showed that ENGs are highly expressed in part of neutrophil cluster (Figure 17C). Remarkably, peritoneal neutrophils of Coch KO mice had higher ENGs expressing neutrophils than those of WT mice (Figure 17D). These data indicate that both neutrophils of WT and Coch KO mice infiltrate to peritoneal cavity but have distinct role after infection. In ENGs, *Chil3*, *Camp*, *Mmp8*, *Ngp* genes are expressed in bone marrow neutrophils. Those genes were also mainly expressed in Coch KO peritoneal neutrophils than WT peritoneal neutrophils. Violin plot showed significant increase of peritoneal neutrophils from Coch KO mice in *Chil3*, *Camp*, *Mmp8*, *Ngp* genes than WT mice (Figure 18A). To confirm expression pattern of ENGs in other sites, I isolated neutrophils from bone marrow, blood, and PLF. Since neutrophils were few in peritoneal cavity before infection, only bone marrow, blood derived neutrophils were analyzed as control group.

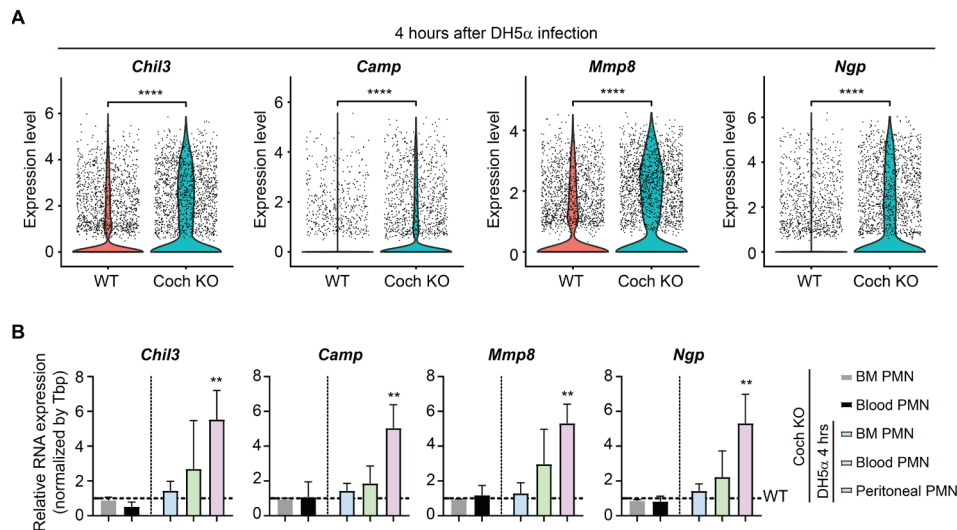


**Figure 18. Early neutrotime genes (ENGs) are up-regulated in the peritoneal neutrophils of Coch KO male mice after DH5 $\alpha$  infection. (A)** Violin plot of *Chil3*, *Camp*, *Mmp8*, *Ngp* expression level between WT and Coch KO peritoneal neutrophils. Each dots represented gene expression level of neutrophils. (B) Representative data of qRT-PCR for *Chil3*, *Camp*, *Mmp8*, *Ngp* expression level between WT and Coch KO bone marrow, blood, peritoneal neutrophils (PMN). 3 independent experiments were repeated for statistics. Statistical analysis was performed by student t-test and Mann-Whitney's U test. *P*-value : \*\* <0.01, \*\*\*\* <0.0001.

Expression of *Chil3*, *Camp*, *Mmp8*, *Ngp* genes had no significant difference in bone marrow, blood derived neutrophils. However, peritoneal neutrophils had 5-fold increase in *Chil3*, *Camp*, *Mmp8*, *Ngp* genes of Coch KO mice than WT mice (Figure 18B). With qRT-PCR data, I suggested that cochlin deficiency leads to infiltration of ENG<sup>high</sup> neutrophils in peritoneal cavity during systemic inflammation.

### **3.6. Neutrophils from ENG<sup>low</sup> clusters that express *Cxcr2* accumulate in the peritoneal cavity, which is induced by cochlin LCCL peptide**

Next, I validated differentially expressed genes (DEGs) in ENG<sup>high</sup> and ENG<sup>low</sup> neutrophils in WT and Coch KO mice. As expected, ENG<sup>high</sup> neutrophils in Coch KO mice were expressing *Ngp* gene (Figure 19A). On the contrary, ENG<sup>low</sup> neutrophils in WT mice were expressing *Ccl6*, *Csf3r*, and *Cxcr2* known as mature inflammatory neutrophil phenotypes (Figure 19B). Especially, CXCR2 is a co-receptor of ligand CXCL1 and CXCL2 involves in neutrophil chemotaxis at acute inflammation<sup>39</sup>. Previously, CXCL1 and CXCL2 protein expression were elevated in sera of WT mice than Coch KO mice in my data (Figure 4, Figure 10). Through single-cell RNA sequencing data, ENG<sup>high</sup> neutrophils might have lower expression of *Cxcr2* with less accumulation in peritoneal cavity.

To verify surface CXCR2 expression level of neutrophils in blood and PECs, I performed flow cytometry. The results showed that CXCR2 expressed blood and peritoneal neutrophils from WT mice had no difference compared to Coch KO mice at 4 hours after infection. In addition, CXCR4, known as marker of aged neutrophils, was no different between WT and Coch KO mice peritoneal neutrophils either. Interestingly, expression of CXCR2 in blood and peritoneal neutrophils were more expressed in WT mice compared to Coch KO mice (Figure 20A, B). Generally, highly activated, infiltrated neutrophils are characterized by low CXCR1 and CXCR2 expression levels<sup>40</sup>.

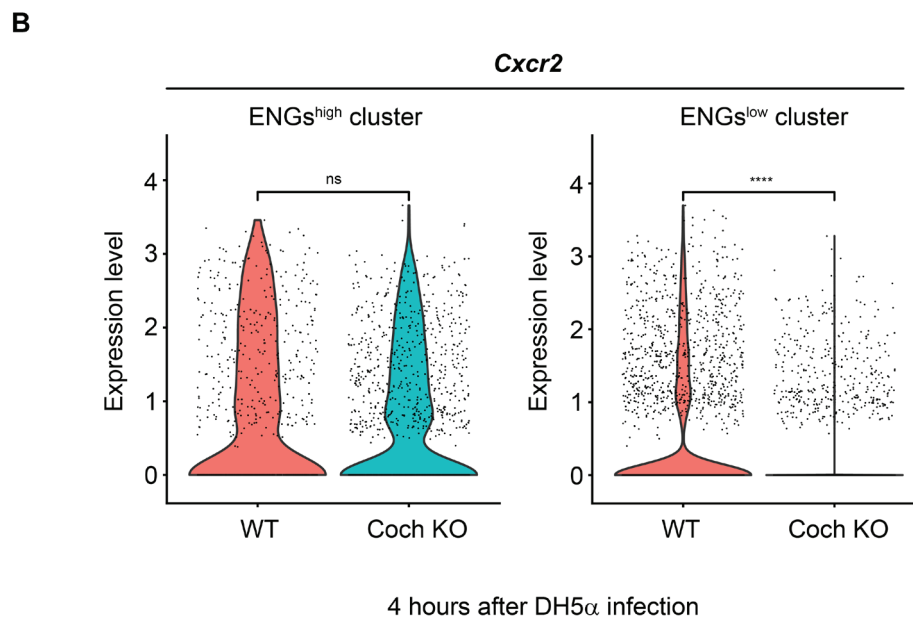
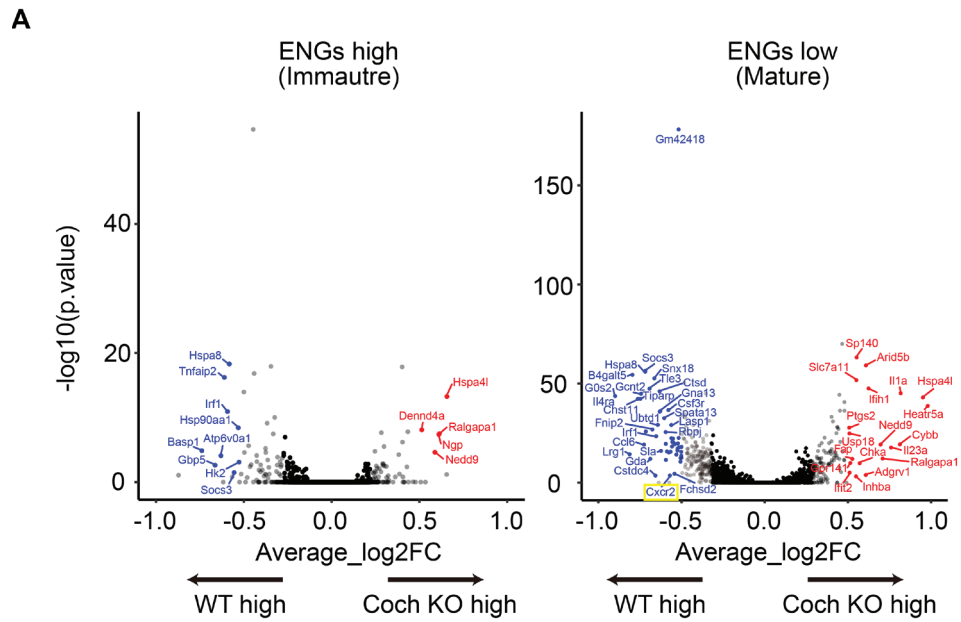


**Figure 19. Peritoneal neutrophils of ENG<sup>+</sup> low cluster from WT male mice exhibit higher expression of *Cxcr2* after DH5 $\alpha$  infection .** (A) Volcano plot of differentially expressed genes (DEGs) between ENG high and ENG low cluster. The yellow box indicated the interested gene in the low clusters of WT ENG. (B) Violin plot of *Cxcr2* expression in ENG high and low clusters between WT and Coch KO mice. Each dots represented gene expression level of neutrophils. Statistical analysis was performed by student t-test. *P*-value : \*\*\*\* <0.0001.

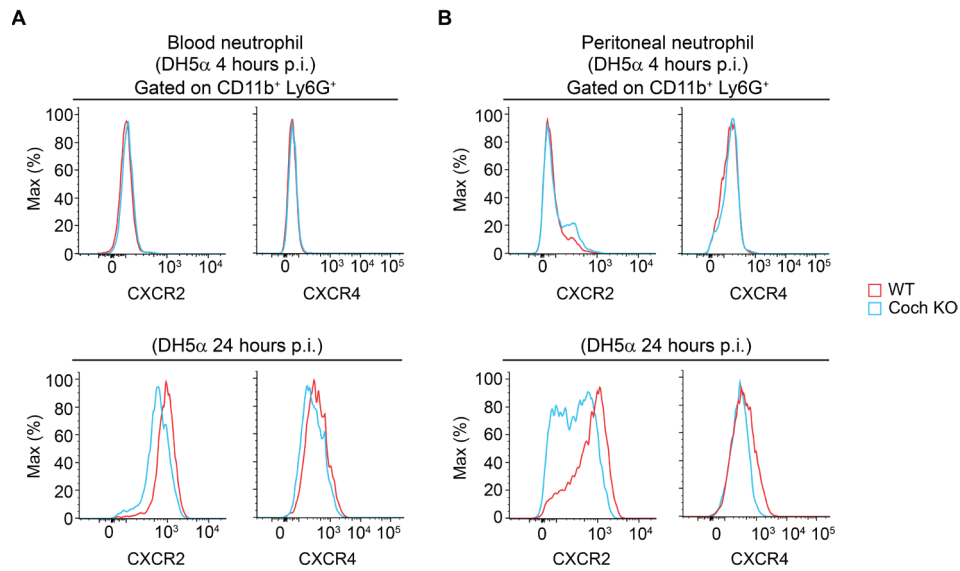


**Figure 20. Neutrophils with high expression of CXCR2 are dominant in WT male mice 24 hours after DH5 $\alpha$  infection.** (A) Histogram of CXCR2, CXCR4 expression level in blood neutrophils. (B) Histogram of CXCR2, CXCR4 expression level in peritoneal neutrophils. Neutrophils (CD11b<sup>+</sup> Ly6G<sup>+</sup>) were gated at about 10,000 cells per samples. 2 independent flow cytometry was conducted for presenting graph.

However, CXCR2 expression was significantly higher in peritoneal neutrophils from WT mice 24 hours after infection (Figure 20B). The expression level of CXCR4 remained unchanged 24 hours after infection, similar to data obtained 4 hours after infection. Combining the results, I suggested that CXCR2<sup>high</sup> neutrophils are more infiltrated to peritoneal cavity with LCCL peptide dependent manner after DH5 $\alpha$  infection.

### **3.7. The infiltration of CXCR2<sup>high</sup> neutrophils into the peritoneal cavity exacerbates the inflammatory condition in WT mice compared to Coch KO mice**

Then, I hypothesized that accumulation of CXCR2<sup>high</sup> neutrophils was related to prolong proinflammatory states and tissue damage. To elucidate the effects of LCCL peptide in neutrophil, I finally performed western blot to confirm the NETs. In my previous data, over the 70% of the PECs were the neutrophils at 24 hours after DH5 $\alpha$  infection (Figure 12B). Isolated peritoneal neutrophils from WT and Coch KO mice showed that chil3 protein was abundant in Coch KO peritoneal neutrophils. Myeloid peroxidase (MPO) was no different between WT and Coch KO peritoneal neutrophils. However, CitH3, as final product of NETosis, was dramatically expressed in peritoneal neutrophils from WT mice (Figure 21). These results indicate that CXCR2<sup>high</sup> neutrophils may be infiltrated to peritoneal cavity by LCCL peptide after inflammation continues. Previous studies showed that expression of CXCR2 in infiltrated neutrophils was related to promote NETosis<sup>41,42</sup>. Accumulation of CXCR2<sup>high</sup> neutrophils can block the resolution of inflammation via NETosis in peritoneal cavity. Since the excessive CitH3 in tissue after infection can cause damage to a host, I assumed that the mouse dies without recovering from the tissue damage. (Figure 9B, Figure 11). Data indicate that peritoneal neutrophils infiltrated with high levels of CXCR2 can induce NETosis, thereby exacerbating inflammation.

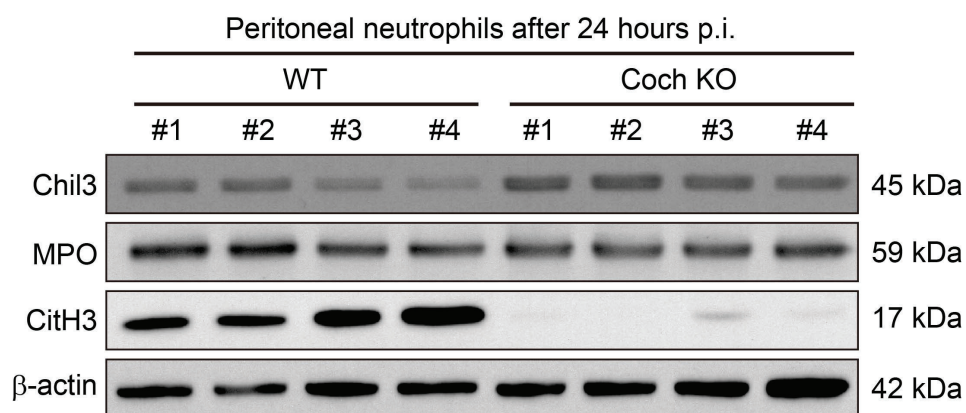


**Figure 21. Infiltrated peritoneal neutrophils from WT male mice cause NETosis 24 hours after DH5 $\alpha$  infection.** Representative western blotting data of peritoneal neutrophils 24 hours after DH5 $\alpha$  infection. 4 independent samples were used (#1~#4). 10 and 12% tris-glycine gel were used for SDS-PAGE. 20  $\mu$ g of peritoneal neutrophil lysate was used for sampling. Membranes were stripped after detection for reblotting.

#### IV. DISCUSSION

In previous studies, cochlin LCCL peptide was found to be essential for bacterial clearance in the lung, skin, and inner ear and survival<sup>13-15</sup>. However, in my peritonitis model, cochlin LCCL peptide exacerbates the proinflammatory status through the induction of various cytokines and chemokines. mRNA expression level of chemokines and proinflammatory cytokines of bone marrow and spleen was suppressed in Coch KO mice (Figure 3). Especially, IL-6, CXCL1, and CXCL2 are down-regulated in both LPS-induced and DH5 $\alpha$  infected Coch KO mice (Figure 4, Figure 10). Those cytokines and chemokines are highly produced in endothelial cells and resident macrophages<sup>43-45</sup>.

In the peritoneal cavity, resident macrophages referred to as LPM are dominant and conduct immune surveillance. Besides, B1a cells serve as secretors of natural antibodies (NAbs) that neutralize a wide range of pathogens before triggering the adaptive immune response<sup>18,46</sup>. Once trauma or peritoneal inflammation occurs, localized peritoneal macrophages (LPMs) undergo pyroptosis. This process involves the expression of IL-1 $\beta$  and IL-18, forming aggregates along with B1a cells and recruited neutrophils in the peritoneum<sup>18</sup>. In Figure 12C and D, my results demonstrated a reduced level of LPMs and myeloid mononuclear cells, including SPMs, post-infection. Nevertheless, bacterial clearance did not differ between WT and Coch KO mice 8 hours after infection, but it was only observed at early time points (2 hours, 4 hours) (Figure 7C). Combining my results, it appears that cochlin LCCL peptide may

influence the phagocytic function of resident macrophages at early time points; however, recruited neutrophils subsequently clear bacteria (Figure 8). In this process, numerous cytokines and chemokines are secreted in order to recruit more myeloid cells. As mentioned above, IL-6 is known to be involved in the initial recruitment of neutrophils and the continuous recruitment of monocytes at the infection site<sup>47</sup>. Moreover, CXCL1 and CXCL2 are major chemokines that interact with CXCR2, which is one of the G protein-coupled receptors (GPCRs)<sup>48,49</sup>.

Recent studies show that expression changes of CXCR2 in neutrophils are related to maturation and activation<sup>50,51</sup>. In acute inflammation, the expression of CXCR2 is initially decreased in the blood but increases again following specific stimulation, such as lipocalin-2<sup>52-55</sup>. In another case, the severity of COVID-19 has been found to alter CXCR2 expression<sup>56</sup>. Numerous studies indicate that impaired outcomes have been observed due to the excessive infiltration of CXCR2-positive neutrophils into tissue<sup>56,57</sup>.

In my study, neutrophils were recruited to the peritoneal cavity regardless of cochlin LCCL peptide (Figure 12B). However, I found different subsets of infiltrating neutrophils between WT and Coch KO mice using single-cell RNA sequencing. The concept of the neutrotime gene is a novel method for separating the step of neutrophils by maturity. Especially, early neutrotime genes (ENGs) are more abundantly expressed in mature bone marrow neutrophils than in mature blood neutrophils<sup>38</sup>. In homeostasis, mature blood

neutrophils circulate throughout the entire body to defend against various pathogens and respond to stimuli. Meanwhile, neutrophils can migrate from the bone marrow to the blood in an immature state during acute inflammation<sup>36</sup>. These immature neutrophils are not fully understood yet; however, recent studies suggest that they possess superior antibacterial capacity and function as granulocyte-like myeloid-derived suppressor cells (G-MDSCs)<sup>58,59</sup>.

In my data, there was a high abundance of relatively immature neutrophils, referred to as  $ENG^{\text{high}}$  subsets, in the peritoneal cavity of Coch KO mice. On the other hand, WT mice showed  $ENG^{\text{low}}$  neutrophil infiltration in the peritoneal cavity, as demonstrated in Figure 17D and Figure 18. It is still unclear how cochlin LCCL peptide regulates the egression of neutrophils from the bone marrow to the blood, but a recent discovery suggests a potential association between cochlin LCCL peptide and the maturation and polarization of neutrophils involving the expression of CXCR2. The expression of CXCR2 in neutrophils may have decreased at 4 hours after infection in both WT and Coch KO mice, suggesting that the CXCR2 level was down-regulated following bone marrow egression and the initiation of inflammation. However, 24 hours after infection, infiltrated  $CXCR2^{\text{high}}$  peritoneal neutrophils were dominant in WT mice compared to Coch KO mice (Figure 20). Therefore, WT mice have relatively more disease phenotype of  $CXCR2^{\text{high}}$  peritoneal neutrophil infiltration, despite CXCR2 expression diminishing in the tissues after severe inflammation. In this process, activated and polarized neutrophils can migrate

into tissues, exacerbating the damage caused by degranulation and excessive cell death. In Figure 6, using two-photon microscopy, I observed robust adhesion and amoeboid migration of neutrophils in the omentum interstitial tissue of WT mice. Although more studies are needed to demonstrate a direct relationship between adhesion and tissue damage, there are significant advantages to revealing migration patterns and cell death *in vivo*.

Recent studies show that the expression of CXCR2 in infiltrated neutrophils is related to promoting NETosis<sup>60-62</sup>. In addition, blocking CXCR2 with an antagonist or monoclonal antibody is known to attenuate inflammatory disorders such as arthritis and atopic dermatitis<sup>63</sup>. Cochlin LCCL peptide derived CXCR2<sup>high</sup> neutrophil infiltration results in excessive CitH3 production induced by NETosis (Figure 21). Furthermore, the degranulation and necrotic cell death of CXCR2<sup>high</sup> neutrophils may cause irreversible detrimental effects to the host organ. On the contrary, Coch KO mice might initially exhibit immune resistance, but eventually develop immune tolerance that renders them unresponsive to self-antigens in order to prevent damage to the host<sup>64</sup>.

Knocking out the entire body of cochlin in mice can impact the developmental process of immunity. Therefore, inhibiting the production of cochlin might be useful in studying the intact function of cochlin LCCL peptide, thereby overcoming those limitations. Aggrecanase I, which is encoded by *Adamts4*, is known to cleave the N-terminal part of cochlin in order to produce the LCCL peptide<sup>13</sup>. In the previous study, it was found that *Adamts4* can be

blocked by tissue inhibitor of metalloproteinase 3 (TIMP-3)<sup>65</sup>. Otherwise, a high dose of an *Adamts5* inhibitor can block the function of *Adamts4* both *in vitro* and *in vivo*<sup>66</sup>. The use of a blockade is expected to reduce the immunological difference caused by the gap in cochlin production among WT mice.

While my previous results are specific to male mice, I believe it is important to also study the effects of LCCL peptide in female mice. Numerous previous studies show sex-hormone dependent modulation of peritoneal cells. Especially, peritoneal macrophages in female mice express higher levels of toll-like receptor (TLR) 2 and 4, which are related to pathogen recognition, compared to male mice. However, recruitment of peritoneal neutrophils is not as effective in female mice compared to male mice<sup>26</sup>. Further research is still required to thoroughly understand the gender-specific function of the LCCL peptide in these processes. Finally, it is believed that managing excessive inflammation, as well as controlling the response to LCCL peptide, is crucial to attenuate systemic inflammation.

## V. CONCLUSION

I have found that LCCL peptide enhances the inflammatory response, particularly in male mice, targeting the elimination of bacteria. However, the excessive presence of inflammatory cytokines and chemokines can lead to a cytokine storm, which attacks the organs of the host. Resident macrophages in the peritoneal cavity are initially involved in phagocytosis to elevate cytokine and chemokine expression. Cochlin deficiency may affect the function of resident macrophages and other immune cells, leading to a decrease in their ability to engulf bacteria. Despite delayed bacterial clearance and low cytokine expression, Coch KO mice catch up with WT mice, followed by neutrophil infiltration. In this procedure, Coch KO mice recruit a more immature subset of neutrophils. This immature and mature subset is distinguished using single-cell RNA sequencing based on early neutrotome genes (ENGs). Coch KO mice have a predominance of relatively immature neutrophils called  $ENG^{high}$  peritoneal neutrophils. However,  $ENG^{low}$  peritoneal neutrophils can express high levels of *Cxcr2* in WT mice. In WT mice,  $CXCR2^{high}$  neutrophils are recruited more in the late stage of infection at the peritoneal cavity. During this process, the generation of NETs by  $CXCR2^{high}$  peritoneal neutrophils is confirmed by CitH3 expression. Circulating CitH3 might induce excessive tissue damage. Uncontrolled composite immune response occurs in WT mice due to cochlin LCCL peptide during infection. Therefore, regulating cochlin LCCL peptide in the context of systemic inflammation shows promise as a therapeutic target.

## REFERENCES

1. Huber-Lang M, Lambris JD, Ward PA. Innate immune responses to trauma. *Nature Immunology* 2018;19:327-41.
2. Cho Y, Hawley CM, Johnson DW. Clinical causes of inflammation in peritoneal dialysis patients. *Int J Nephrol* 2014;2014:909373.
3. Yang Y, Xu Y, Liu S, Lu P, Zhou H, Yang M. The systemic inflammation indexes predict all-cause mortality in peritoneal dialysis patients. *Renal Failure* 2023;45:2160348.
4. Beltrán MA. The Systemic Inflammatory Response in Patients with Appendicitis: a Progressive Phenomenon. *Indian J Surg* 2015;77:1050-6.
5. Şener K, Çakır A, Kılavuz H, Altuğ E, Güven R. Diagnostic value of systemic immune inflammation index in acute appendicitis. *Rev Assoc Med Bras (1992)* 2023;69:291-6.
6. Danford CJ, Lin SC, Smith MP, Wolf JL. Encapsulating peritoneal sclerosis. *World J Gastroenterol* 2018;24:3101-11.
7. Moinuddin Z, Summers A, Van Dellen D, Augustine T, Herrick SE. Encapsulating peritoneal sclerosis-a rare but devastating peritoneal disease. *Front Physiol* 2014;5:470.
8. Yang B, Zhang G, Elias M, Zhu Y, Wang J. The role of cytokine and immune responses in intestinal fibrosis. *J Dig Dis* 2020;21:308-14.

9. Mari A, Abu Backer F, Mahamid M, Amara H, Carter D, Boltin D, et al. Bloating and Abdominal Distension: Clinical Approach and Management. *Adv Ther* 2019;36:1075-84.
10. Hegde S, Lin Y-M, Golovko G, Khanipov K, Cong Y, Savidge T, et al. Microbiota dysbiosis and its pathophysiological significance in bowel obstruction. *Scientific Reports* 2018;8:13044.
11. Zhang C, Yang M. The Role and Potential Application of Antimicrobial Peptides in Autoimmune Diseases. *Front Immunol* 2020;11:859.
12. Huan Y, Kong Q, Mou H, Yi H. Antimicrobial Peptides: Classification, Design, Application and Research Progress in Multiple Fields. *Front Microbiol* 2020;11:582779.
13. Py BF, Gonzalez SF, Long K, Kim MS, Kim YA, Zhu H, et al. Cochlin produced by follicular dendritic cells promotes antibacterial innate immunity. *Immunity* 2013;38:1063-72.
14. Nyström A, Bornert O, Kühl T, Gretzmeier C, Thriene K, Dengjel J, et al. Impaired lymphoid extracellular matrix impedes antibacterial immunity in epidermolysis bullosa. *Proc Natl Acad Sci U S A* 2018;115:E705-e14.
15. Jung J, Yoo JE, Choe YH, Park SC, Lee HJ, Lee HJ, et al. Cleaved Cochlin Sequesters *Pseudomonas aeruginosa* and Activates Innate Immunity in the Inner Ear. *Cell Host Microbe* 2019;25:513-25.e6.

16. Cassado Ados A, D'Império Lima MR, Bortoluci KR. Revisiting mouse peritoneal macrophages: heterogeneity, development, and function. *Front Immunol* 2015;6:225.
17. Buscher K, Wang H, Zhang X, Striewski P, Wirth B, Saggi G, et al. Protection from septic peritonitis by rapid neutrophil recruitment through omental high endothelial venules. *Nat Commun* 2016;7:10828.
18. Vega-Pérez A, Villarrubia LH, Godio C, Gutiérrez-González A, Feo-Lucas L, Ferriz M, et al. Resident macrophage-dependent immune cell scaffolds drive anti-bacterial defense in the peritoneal cavity. *Immunity* 2021;54:2578-94.e5.
19. Deng Q, Pan B, Alam HB, Liang Y, Wu Z, Liu B, et al. Citrullinated Histone H3 as a Therapeutic Target for Endotoxic Shock in Mice. *Front Immunol* 2019;10:2957.
20. Tian Y, Li P, Wu Z, Deng Q, Pan B, Stringer KA, et al. Citrullinated Histone H3 Mediates Sepsis-Induced Lung Injury Through Activating Caspase-1 Dependent Inflammasome Pathway. *Front Immunol* 2021;12:761345.
21. Faust N, Varas F, Kelly LM, Heck S, Graf T. Insertion of enhanced green fluorescent protein into the lysozyme gene creates mice with green fluorescent granulocytes and macrophages. *Blood* 2000;96:719-26.

22. Park SA, Choe YH, Lee SH, Hyun YM. Two-photon Intravital Imaging of Leukocytes During the Immune Response in Lipopolysaccharide-treated Mouse Liver. *J Vis Exp* 2018; doi:10.3791/57191.
23. Lee SH, Choe YH, Kang RH, Kim YR, Kim NH, Kang S, et al. A bright blue fluorescent dextran for two-photon in vivo imaging of blood vessels. *Bioorg Chem* 2019;89:103019.
24. Hussain S, Stohlman SA. Peritoneal macrophage from male and female SJL mice differ in IL-10 expression and macrophage maturation. *J Leukoc Biol* 2012;91:571-9.
25. Minton K. Peritoneal sex differences. *Nature Reviews Immunology* 2020;20:460-1.
26. Scotland RS, Stables MJ, Madalli S, Watson P, Gilroy DW. Sex differences in resident immune cell phenotype underlie more efficient acute inflammatory responses in female mice. *Blood* 2011;118:5918-27.
27. Bain CC, Gibson DA, Steers NJ, Boufeia K, Louwe PA, Doherty C, et al. Rate of replenishment and microenvironment contribute to the sexually dimorphic phenotype and function of peritoneal macrophages. *Sci Immunol* 2020;5.
28. Dinarello CA. Overview of the IL-1 family in innate inflammation and acquired immunity. *Immunol Rev* 2018;281:8-27.

29. Gabay C, Lamacchia C, Palmer G. IL-1 pathways in inflammation and human diseases. *Nature Reviews Rheumatology* 2010;6:232-41.
30. Park SA, Hyun YM. Neutrophil Extravasation Cascade: What Can We Learn from Two-photon Intravital Imaging? *Immune Netw* 2016;16:317-21.
31. Hyun Y-M, Choe YH, Park SA, Kim M. LFA-1 (CD11a/CD18) and Mac-1 (CD11b/CD18) distinctly regulate neutrophil extravasation through hotspots I and II. *Experimental & Molecular Medicine* 2019;51:1-13.
32. Filippi M-D. Neutrophil transendothelial migration: updates and new perspectives. *Blood* 2019;133:2149-58.
33. Ghosn EE, Cassado AA, Govoni GR, Fukuhara T, Yang Y, Monack DM, et al. Two physically, functionally, and developmentally distinct peritoneal macrophage subsets. *Proc Natl Acad Sci U S A* 2010;107:2568-73.
34. Ng LG, Ostuni R, Hidalgo A. Heterogeneity of neutrophils. *Nat Rev Immunol* 2019;19:255-65.
35. Grieshaber-Bouyer R, Nigrovic PA. Neutrophil Heterogeneity as Therapeutic Opportunity in Immune-Mediated Disease. *Front Immunol* 2019;10:346.

36. Xie X, Shi Q, Wu P, Zhang X, Kambara H, Su J, et al. Single-cell transcriptome profiling reveals neutrophil heterogeneity in homeostasis and infection. *Nat Immunol* 2020;21:1119-33.
37. Furze RC, Rankin SM. Neutrophil mobilization and clearance in the bone marrow. *Immunology* 2008;125:281-8.
38. Grieshaber-Bouyer R, Radtke FA, Cunin P, Stifano G, Levescot A, Vijaykumar B, et al. The neutrotime transcriptional signature defines a single continuum of neutrophils across biological compartments. *Nature Communications* 2021;12:2856.
39. Raghuwanshi SK, Su Y, Singh V, Haynes K, Richmond A, Richardson RM. The chemokine receptors CXCR1 and CXCR2 couple to distinct G protein-coupled receptor kinases to mediate and regulate leukocyte functions. *J Immunol* 2012;189:2824-32.
40. Metzemaekers M, Gouwy M, Proost P. Neutrophil chemoattractant receptors in health and disease: double-edged swords. *Cell Mol Immunol* 2020;17:433-50.
41. Alsabani M, Abrams ST, Cheng Z, Morton B, Lane S, Alosaimi S, et al. Reduction of NETosis by targeting CXCR1/2 reduces thrombosis, lung injury, and mortality in experimental human and murine sepsis. *Br J Anaesth* 2022;128:283-93.
42. Teijeira A, Garasa S, Gato M, Alfaro C, Migueliz I, Cirella A, et al. CXCR1 and CXCR2 Chemokine Receptor Agonists Produced by

- Tumors Induce Neutrophil Extracellular Traps that Interfere with Immune Cytotoxicity. *Immunity* 2020;52:856-71 e8.
43. Arango Duque G, Descoteaux A. Macrophage cytokines: involvement in immunity and infectious diseases. *Front Immunol* 2014;5:491.
  44. Mantovani A, Sica A, Sozzani S, Allavena P, Vecchi A, Locati M. The chemokine system in diverse forms of macrophage activation and polarization. *Trends Immunol* 2004;25:677-86.
  45. Mai J, Virtue A, Shen J, Wang H, Yang XF. An evolving new paradigm: endothelial cells--conditional innate immune cells. *J Hematol Oncol* 2013;6:61.
  46. Catala C, Velasco-de Andres M, Casado-Llombart S, Leyton-Pereira A, Carrillo-Serradell L, Isamat M, et al. Innate immune response to peritoneal bacterial infection. *Int Rev Cell Mol Biol* 2022;371:43-61.
  47. Kaplanski G, Marin V, Montero-Julian F, Mantovani A, Farnarier C. IL-6: a regulator of the transition from neutrophil to monocyte recruitment during inflammation. *Trends Immunol* 2003;24:25-9.
  48. Sawant KV, Sepuru KM, Lowry E, Penaranda B, Frevert CW, Garofalo RP, et al. Neutrophil recruitment by chemokines Cxcl1/KC and Cxcl2/MIP2: Role of Cxcr2 activation and glycosaminoglycan interactions. *J Leukoc Biol* 2021;109:777-91.

49. Boro M, Balaji KN. CXCL1 and CXCL2 Regulate NLRP3 Inflammasome Activation via G-Protein-Coupled Receptor CXCR2. *J Immunol* 2017;199:1660-71.
50. Delobel P, Ginter B, Rubio E, Balabanian K, Lazenec G. CXCR2 intrinsically drives the maturation and function of neutrophils in mice. *Front Immunol* 2022;13:1005551.
51. Martin C, Burdon PC, Bridger G, Gutierrez-Ramos JC, Williams TJ, Rankin SM. Chemokines acting via CXCR2 and CXCR4 control the release of neutrophils from the bone marrow and their return following senescence. *Immunity* 2003;19:583-93.
52. Ye D, Yang K, Zang S, Lin Z, Chau HT, Wang Y, et al. Lipocalin-2 mediates non-alcoholic steatohepatitis by promoting neutrophil-macrophage crosstalk via the induction of CXCR2. *J Hepatol* 2016;65:988-97.
53. Rios-Santos F, Alves-Filho JC, Souto FO, Spiller F, Freitas A, Lotufo CM, et al. Down-regulation of CXCR2 on neutrophils in severe sepsis is mediated by inducible nitric oxide synthase-derived nitric oxide. *Am J Respir Crit Care Med* 2007;175:490-7.
54. Hu N, Westra J, Rutgers A, Doornbos-Van der Meer B, Huitema MG, Stegeman CA, et al. Decreased CXCR1 and CXCR2 expression on neutrophils in anti-neutrophil cytoplasmic autoantibody-associated

vasculitides potentially increases neutrophil adhesion and impairs migration. *Arthritis Res Ther* 2011;13:R201.

rs migration. *Arthritis Res Ther* 2011;13:R201.

55. Del Rio L, Bennouna S, Salinas J, Denkers EY. CXCR2 deficiency confers impaired neutrophil recruitment and increased susceptibility during *Toxoplasma gondii* infection. *J Immunol* 2001;167:6503-9.
56. Rice CM, Lewis P, Ponce-Garcia FM, Gibbs W, Groves S, Cela D, et al. Hyperactive immature state and differential CXCR2 expression of neutrophils in severe COVID-19. *Life Sci Alliance* 2023;6.
57. Liu N, Bauer M, Press AT. The immunological function of CXCR2 in the liver during sepsis. *J Inflamm (Lond)* 2022;19:23.
58. Hong CW. Current Understanding in Neutrophil Differentiation and Heterogeneity. *Immune Netw* 2017;17:298-306.
59. van Grinsven E, Textor J, Hustin LSP, Wolf K, Koenderman L, Vrisekoop N. Immature Neutrophils Released in Acute Inflammation Exhibit Efficient Migration despite Incomplete Segmentation of the Nucleus. *J Immunol* 2019;202:207-17.
60. Marcos V, Zhou Z, Yildirim AO, Bohla A, Hector A, Vitkov L, et al. CXCR2 mediates NADPH oxidase-independent neutrophil extracellular trap formation in cystic fibrosis airway inflammation. *Nat Med* 2010;16:1018-23.

61. Safarulla S, Madan A, Xing F, Chandrasekaran A. CXCR2 Mediates Distinct Neutrophil Behavior in Brain Metastatic Breast Tumor. *Cancers (Basel)* 2022;14.
62. Teixeira A, Garasa S, Ochoa MDC, Cirella A, Olivera I, Glez-Vaz J, et al. Differential Interleukin-8 thresholds for chemotaxis and netosis in human neutrophils. *Eur J Immunol* 2021;51:2274-80.
63. Alam MJ, Xie L, Ang C, Fahimi F, Willingham SB, Kueh AJ, et al. Therapeutic blockade of CXCR2 rapidly clears inflammation in arthritis and atopic dermatitis models: demonstration with surrogate and humanized antibodies. *MAbs* 2020;12:1856460.
64. McCarville JL, Ayres JS. Disease tolerance: concept and mechanisms. *Curr Opin Immunol* 2018;50:88-93.
65. Fan D, Kassiri Z. Biology of Tissue Inhibitor of Metalloproteinase 3 (TIMP3), and Its Therapeutic Implications in Cardiovascular Pathology. *Front Physiol* 2020;11:661.
66. Santamaria S, Cuffaro D, Nuti E, Ciccone L, Tuccinardi T, Liva F, et al. Exosite inhibition of ADAMTS-5 by a glycoconjugated arylsulfonamide. *Sci Rep* 2021;11:949.

## ABSTRACT(IN KOREAN)

복막염 유발 마우스에서 cochlin LCCL 도메인에 의한 선천성  
면역세포 이질성과 세균 사멸 조절 기전 규명

<지도교수 현 영 민>

연세대학교 대학원 의과학과

최 영 호

복막과 복강은 외부의 감염으로부터 장기들을 보호하는 데 중요한 장벽들이다. 복강에는 대식세포나 림프세포와 같은 다양한 내재 면역세포들이 떠돌아다니며 외래의 물질들을 탐지한다. 박테리아 감염이나 외상에 의한 염증반응이 발생하면, 내재 대식세포들이 병원균들을 제거하고 선천성 면역세포들이 유입되어 추가적인 작업을 진행한다. 이 과정에서 다양한 항박테리아 물질들이 복강 면역에 관여한다. 그 중 Cochlin은 기존 보고에 따르면 내이와 전정기관에서 발견된다고 알려져 있는데, 비장과 림프샘과 같은 2차 림프 기관에서도 존재하는 것이 최근 연구들에서 발견되었다. Cochlin은 전신성 염증반응이 발생하면 LCCL 펩타이드로 잘려져 혈류로 유입이

된다. 하지만 선천성 면역에서 잘린 LCCL 펩타이드의 기능이 아직 잘 연구되어 있지 않았다. 본 연구를 통해, 나는 LCCL 펩타이드가 복강에서의 초기 대식 작용과 친 염증성 사이토카인의 조절에 중요한 역할을 한다는 것을 확인하였다. 하지만 LCCL 펩타이드는 지속적인 사이토카인 폭풍에 의한 장기부전을 일으켜 치사율을 증가시키기도 한다. 단일 세포 RNA 시퀀싱을 통해, 우리는 초기 호중구 유전자들이 Cochlin 결여 호중구들에서 높게 발현되는 것을 확인하였다. 초기 호중구 유전자들은 Chil3, Camp, Mmp8와 Ngp같은 유전자들을 포함하는 미성숙 호중구에서 발현되는 특징을 가진다. 본 연구모델에서, Cochlin이 결여된 마우스의 호중구들이 더 적은 염증반응과 호중구 세포 밖 덩어리를 적게 생성하는 것을 확인하였다. 반면에, 대조군 호중구는 CXCR2 수용체를 통해 CXCL1과 CXCL2에 반응하여 친 염증성 특징을 가지는 세포들이 상당한 것으로 보였다. 결론적으로 LCCL 펩타이드는 CXCR2 수용체 발현이 높고 Chil3 발현이 낮은 호중구들을 유입시켜 박테리아를 제거하게 하지만 이러한 유입이 결과적으로 호중구 세포 밖 덩어리를 형성하여 염증반응이 지속되었을 때 숙주에게 피해를 줄 수도 있음을 연구하였다.

---

핵심되는 말 : Cochlin, LCCL 도메인, 선천성 면역, 호중구, 대식세포, 복막염, 대장균, 감염, 단일 세포 RNA 시퀀싱, 호중구 세포 밖 덩어리

## PUBLICATION LIST

1. Park SA, **Choe YH**, Lee SH, Hyun YM. Two-photon Intravital Imaging of Leukocytes During the Immune Response in Lipopolysaccharide-treated Mouse Liver. *J Vis Exp* 2018; doi:10.3791/57191.
2. Lee SH, **Choe YH**, Kang RH, Kim YR, Kim NH, Kang S, et al. A bright blue fluorescent dextran for two-photon in vivo imaging of blood vessels. *Bioorg Chem* 2019;89:103019.
3. Jung J, Yoo JE, **Choe YH**, Park SC, Lee HJ, Lee HJ, et al. Cleaved Cochlin Sequesters *Pseudomonas aeruginosa* and Activates Innate Immunity in the Inner Ear. *Cell Host Microbe* 2019;25:513-25.e6.